Theoretical Ecology (2024) 17:203–234
https://doi.org/10.1007/s12080-024-00585-5

RESEARCH

The dynamics of evolutionary branching in an ecological model

Roger Cropp[1] · **John Norbury**[2]

Received: 28 June 2023 / Accepted: 8 June 2024 / Published online: 8 July 2024

Abstract
Eco-evolutionary modelling involves the coupling of ecological equations to evolutionary ones. The interaction between ecological dynamics and evolutionary processes is essential to simulating evolutionary branching, a precursor to speciation. The creation and maintenance of biodiversity in models depends upon their ability to capture the dynamics of evolutionary branching. Understanding these systems requires low-dimension models that are amenable to analysis. The rapid reproduction rates of marine plankton ecosystems and their importance in determining the fluxes of climatically important gases between the ocean and atmosphere suggest that the next generation of global climate models needs to incorporate eco-evolutionary models in the ocean. This requires simple population-level models, that can represent such eco-evolutionary processes with orders of magnitude fewer equations than models that follow the dynamics of individual phenotypes. We present a general framework for developing eco-evolutionary models and consider its general properties. This framework defines a fitness function and assumes a beta distribution of phenotype abundances within each population. It simulates the change in total population size, the mean trait value, and the trait differentiation, from which the variance of trait values in the population may be calculated. We test the efficacy of the eco-evolutionary modelling framework by comparing the dynamics of evolutionary branching in a six-equation eco-evolutionary model that has evolutionary branching, with that of an equivalent one-hundred equation model that simulates the dynamics of every phenotype in the population. The latter model does not involve a population fitness function, nor does it assume a distribution of phenotype abundance across trait values. The eco-evolutionary population model and the phenotype model produce similar evolutionary branching, both qualitatively and quantitatively, in both symmetric and asymmetric fitness landscapes. In order to better understand the six-equation model, we develop a heuristic three-equation eco-evolutionary model. We use the density-independent mortality parameter as a convenient bifurcation parameter, so that differences in evolutionary branching dynamics in symmetric and asymmetric fitness landscapes may be investigated. This model shows that evolutionary branching of a stable population is flagged by a zero in the local trait curvature; the trait curvature then changes sign from negative to positive and back to negative, along the solution. It suggests that evolutionary branching points may be generated differently, with different dynamical properties, depending upon, in this case, the symmetry of the system. It also suggests that a changing environment, that may change attributes such as mortality, could have profound effects on an ecosystem's ability to adapt. Our results suggest that the properties of the three-dimensional model can provide useful insights into the properties of the higher-dimension models. In particular, the bifurcation properties of the simple model predict the processes by which the more complicated models produce evolutionary branching points. The corresponding bifurcation properties of the phenotype and population models, evident in the dynamics of the phenotype distributions they predict, suggest that our eco-evolutionary modelling framework captures the essential properties that underlie the evolution of phenotypes in populations.

Keywords Evolutionary branching · Eco-evolutionary population modelling framework · Trait adaptation · Biodiversity · Trait differentiation

✉ Roger Cropp
r.cropp@griffith.edu.au

[1] School of Environment and Science, Griffith University, Nathan, Queensland 4111, Australia

[2] Mathematical Institute, University of Oxford, Andrew Wiles Building, ROQ, Woodstock Road, Oxford OX2 6GG, UK

Introduction

An understanding of how biological diversity is created and maintained is one of the major challenges facing humanity in its bid to preserve functioning ecosystems on Earth.

The accelerating impact of human activities on ecosystems at all scales, from how bacteria evolve in response to antibiotics to the local impacts of habitat loss and the global impacts of climate change, presents a pressing need for the development of parsimonious models, composed of a few differential equations, that can simulate the dynamics of eco-evolutionary systems and predict the implications of human activities (Irwin et al. 2015; Padfield et al. 2017; Beaufort et al. 2022). The ability of models of evolution to simulate evolutionary branching is a litmus test for realistic eco-evolutionary models.

Evolutionary branching (Metz et al. 1996) is a major contribution of Adaptive Dynamics (AD) (Geritz et al. 1998) to understanding the processes of evolution (Della Rossa et al. 2015; Dercole et al. 2016), and may elucidate a fundamental process in sympatric speciation (Waxman and Gavrilets 2005; Senthilnathan and Gavrilets 2021). Evolutionary branching is the splitting of a unimodal phenotype distribution of a population into a bimodal, or even multimodal phenotype distribution, and is considered to generally occur at an eco-evolutionary equilibrium point that is ecologically stable but evolutionarily unstable (Wakano and Iwasa 2013). Quantitative genetics models consider that evolutionary branching occurs when the trait mean is constant, but the trait variance increases without bound (Mullon and Lehmann 2019), although trait variances may not necessarily be unbounded (Debarre and Otto 2016). The transition at such eco-evolutionary saddle points is sometimes described as "catastrophic" (Dercole et al. 2016), but may not necessarily be so (Wakano and Iwasa 2013).

The dynamics of evolutionary branching may be investigated by simulating large numbers of interacting phenotypes of a population, for example, Geritz et al. (1997, 1998), Law et al. (1997). The AD approach models a single resident phenotype and tests whether a mutant phenotype can invade a convergent stable equilibrium occupied by the resident phenotype - if it cannot be invaded the equilibrium is an evolutionary stable strategy (Dercole et al. 2016).

An alternative to modelling individual phenotypes is to model the population, its average trait value, and a measure of trait variance within the population (Klauschies et al. 2018; Patel and Burger 2019; Lion et al. 2023). Eco-evolutionary models seek to simulate the complex interplay of ecological interactions between populations and the evolutionary processes that shape their characteristics (Abrams et al. 1993; Dieckmann and Law 1996; Dieckmann and Doebeli 1999; Fussman et al. 2007; Pelletier et al. 2009; Schoener 2011; Cortez 2018; Klauschies et al. 2018; Lion et al. 2023). Our framework allows dynamic feedback to occur between the ecology and evolution and *vice versa*. Pelletier et al. (2009) raise the joint feedback issue as a key attribute of eco-evolutionary dynamics.

Eco-evolutionary modelling assumes that ecological and evolutionary processes can occur on similar time scales, and evolutionary dynamics can affect ecology (Schoener 2011; Villa Martin et al. 2016). In 2009 the Philosophical Transactions of the Royal Society B devoted a theme issue to this topic (see the introductory paper of Pelletier et al. (2009)). Eco-evolutionary population models typically involve orders of magnitude fewer equations than their phenotype model equivalents, and examine the dynamics of a system rather than just its steady states or their long-term stable attractors.

A key difference between eco-evolutionary modelling and the AD approach is that all possible mutants are included in the model's initial conditions, so the AD criterion of explicitly testing each stable equilibrium point for invasibility by a mutant is redundant, as this has already been done in arriving at the equilibrium. As a result, the criteria for evolutionary branching developed by AD (Waxman and Gavrilets 2005) are generally not directly applicable to eco-evolutionary models.

Branching points in eco-evolutionary models may be characterised as equilibrium points on the fitness landscape where the population fitness is zero, the fitness gradient in the evolutionary dimension is zero, and the curvature of the fitness surface in the evolutionary dimension is positive. Such equilibrium points have attracting eigenvectors in the ecological direction and repelling eigenvectors in the evolutionary direction (Rubin et al. 2021).

Eco-evolutionary models typically have frequency-dependent measures of fitness, considered to be essential to modelling evolutionary dynamics (Metz et al. 1992), that are derived directly from the ecological dynamics. Early eco-evolutionary models often assumed that traits were normally distributed with constant variance (Lande 1976), but phenotype models typically simulate the change in both the mean and variance of traits (Meszena et al. 2005; Senthilnathan and Gavrilets 2021). Many modelling approaches, such as quantitative genetics (Abrams 2001) and oligomorphic dynamics (Sasaki and Dieckmann 2011; Lion et al. 2023), assume sub-populations with unimodal distributions with small variances. Often, phenotypes are assumed to be normally distributed; normal distributions have zero skewness and are often assumed to have constant variance.

Recent eco-evolutionary modelling approaches have explored the possibility that traits may be described by beta distributions, that have dynamic variance and may be skewed or even bimodal (Klauschies et al. 2018). The eco-evolutionary framework used in this paper (Cropp and Norbury 2021, 2022), that follows how the beta distribution changes its shape properties, allows for increases in variance (in the absence of mutation), skewness, and bimodal phenotype distributions, suggesting the potential to simulate evolutionary branching in an eco-evolutionary model.

Here, we examine the dynamical evolutionary branching behaviour of an eco-evolutionary system described by six coupled ordinary differential equations based on an eco-evolutionary framework that assumes phenotypes have beta distributions (see equations (6)-(8) for the specific model and equations (34) in Appendix "Extended eco-evolutionary population modelling framework" section for the general framework). The model simulates the evolution of an autotroph population that trades-off maximising its growth rate against intra-population competition, where the competition between similar phenotypes is greater than that between dissimilar phenotypes. The population trade-off is analogous to that used in some phenotype models (for example, Meszena et al. (2005); Kisdi (1999)), and oligomorphic population models (Lion et al. 2023), so the approach has a similar fitness landscape and related dynamical behaviour.

We develop a two-sub-population ordinary differential equation model, described by six equations, that reproduces the results of an equivalent 100-equation phenotype model with a high level of agreement. A simplified, single population, (three equation) version of the population model has an explicitly three-dimensional fitness landscape. This reveals that weak evolutionary branching is initiated by crossing a zero curvature isocline, prior to strong branching, which is controlled by the unstable manifold of a saddle equilibrium point in the eco-evolutionary state space.

We show that two-dimensional sections through the ecological and evolutionary phase spaces of the two-sub-population model, that change as the system evolves, are useful indicators of the dynamics of the system. Standard dynamical systems analysis tools then provide useful insights into the dynamics of this eco-evolutionary model. For example, they reveal the existence of what may be a lengthy zone where the ecological state is not near equilibrium and/or evolutionary properties of the system may change substantially, confirming the importance of dynamical feedback between ecology and evolution. The phenotype model does not readily provide such insights because of its high dimensionality (typically hundreds of phenotypes).

Pelletier et al. (2009), in their introductory paper to the theme issue "Eco-evolutionary Dynamics" discuss the aims and importance of looking at feedback between the ecological, evolutionary, and environmental systems. Although we do not explicitly model the interaction of environmental forcings in our example, we demonstrate the potential for environmental changes to fundamentally affect the properties of eco-evolutionary systems. This could have profound implications for how major ecosystems, such as coral reefs, adapt to climate change.

The manuscript is organised as follows. We first present a phenotype model that explicitly simulates the dynamics of every phenotype in a population ("A phenotype model with evolutionary branching" section). This model makes no assumptions of fitness functions or trait distributions and serves as a benchmark to compare our model results against. Our eco-evolutionary modelling framework is introduced in the "Modelling framework and a heuristic model" section along with its simplest implementation — a single population model with one evolving trait. This serves as a heuristic model to assist in understanding the properties of the phenotype model and the more complex simulation model. The eco-evolutionary simulation model is introduced in the "A two-sub-population simulation model" section, and the results of simulations in the "Results and discussion" section. This section presents and discusses details of the model's equilibria, its bifurcation behaviours, the role of trait differentiation Q, and analysis of the phase space. A summary of our results is presented in the "Conclusions" section and a comprehensive Appendix provides supporting details of our approach and results.

A phenotype model with evolutionary branching

A common feature of models that exhibit evolutionary branching is that individuals with similar phenotypes compete more strongly with each other than individuals with widely dissimilar phenotypes. An example is beak morphology in birds that determines the size and/or shape of seeds eaten (Grant and Grant 2006). We consider a similar competition model here.

Resource-based ecosystem models of single populations typically contain three ecological processes: growth based on the uptake of a resource; competition between various members of the population; and mortality. Each of these processes may be density-dependent or density-independent, depending upon the specific formulation. A single population model in this framework is typically that of a plant, that technically has density-dependent growth due to resource recycling. Here, we consider a population composed of a number of phenotypes that are differentiated by their value of a trait. This trait determines their relative efficiency at taking up and growing on a resource and how effectively they compete with other phenotypes in the population. The population reproduces continuously and clonally, similarly to phytoplankton.

We define a fitness function, that includes growth, competition, and mortality, for each population P of the form f where the abundance of each phenotype, P_i, changes according to $f(\gamma_i; P_j, \text{ for } 1 \leq j \leq n)$. Each phenotype i is associated with a scaled trait value $0 < \gamma_i < 1$ that determines its maximum growth rate and how it competes with other phenotypes j with scaled trait values γ_j.

We model the competition between phenotypes i in a population whose total size is given by $P = \sum_i P_i$. The phenotype model is given by the equation:

$$\frac{dP_i}{dt} = P_i\left(\frac{\mu\gamma_i(1-\gamma_i)N}{(N+\kappa)} - \sum_j \frac{P_j}{\eta + \omega(\gamma_i-\gamma_j)^2 + \rho(\gamma_i-\gamma_C)^2} - \sigma\right), \tag{1}$$

where the resource N is given by $N = 1 - \sum_i P_i$ and $i, j = 1, 2, \ldots, n$, for n the number of phenotypes simulated. Here the P_i are abundances, measured as the amount of biomass (in terms of scaled limiting resource) in each phenotype, and N is the amount of resource in the abiotic pool. When P is a plant, the resource is a limiting inorganic nutrient.

Each phenotype is subject to the same population-wide density-independent mortality rate σ, as well as the other population parameter values μ, κ, η, ρ, ω, and γ_C. The maximum growth rates of the phenotypes are described by a population growth rate μ, and a concave function of the trait γ such that, for the same availability of resource N, phenotypes with trait values near the middle of the range (i.e. $\gamma_i \approx 0.5$) have greater maximum growth rates than phenotypes with trait values near the bounds ($\gamma_i \approx 0$ or $\gamma_i \approx 1$). The realised growth rate of each phenotype (the first term in (1)) is described by a Michaelis-Menten (Holling Type II) term that modulates (saturates) the maximum possible growth rate of the phenotype $\mu\gamma_i(1-\gamma_i)$ according to the availability of resource. Here, κ represents the half-saturation constant of nutrient uptake, that is, the nutrient concentration at which the organism attains half its maximum growth rate.

Competition between phenotypes is modelled by the second term in equation (1). The first term in the denominator of the competition term η controls the constant, population-wide competition between phenotypes. The second term in the denominator of the competition term, $\omega(\gamma_i-\gamma_j)^2$, reflects that competition between phenotypes with similar trait values is greater than competition between dis-similar phenotypes. The third term in the denominator of the competition term, $\rho(\gamma_i-\gamma_C)^2$, allows differential competition between phenotypes. The parameter $0 < \gamma_C < 1$ identifies a trait value that is detrimental to phenotypes that have it, and to phenotypes with similar trait values. The effect of this trait value on phenotypes' growth decreases for phenotypes with more dissimilar trait values. When the population is small, the effect of this term is minimal, but its effect increases as the population increases. The fitness landscape of (1) is symmetric about $\gamma = 0.5$ when $\gamma_C = 0.5$, but is asymmetric for other values of $0 < \gamma_C < 1$.

Numerical simulations using the phenotype model (1), for given initial conditions and parameter values, with symmetric ($\gamma_C = 0.50$) and asymmetric ($\gamma_C = 0.40$) fitness landscapes with large ($\sigma = 2.00$) and small ($\sigma = 0.50$) density-independent mortality produce the phenotype distributions in Fig. 1. These simulations were initiated with beta-distributed phenotype abundances among the traits, but the results do not depend on this assumption. See Appendix "Phenotype distributions" section for evidence that the model generates beta distributions, even if it does not start with a beta distribution.

Figure 1 shows that for small values of σ ((b) and (d)) the single initial population splits into two sub-populations with different trait means, of equal biomass sizes in the symmetric case and unequal sizes in the asymmetric case. For large values of σ ((a) and (c)) the population remains a single population with a trait mean of 0.50 in the symmetric case, and a trait mean of 0.53 in the asymmetric case. In all cases the variance is small. Note $P_i(t)/\sum_j P_j(t)$ is used as the probability density function to calculate the phenotype statistics.

The asymmetry of the fitness landscape does not noticeably affect the simulation results for large σ ((a) and (c)) but causes the system to produce a larger and a smaller sub-population in the asymmetric branching case (d). The stability and co-existence of the large and small sub-populations in the asymmetric case is due to the competition term $\omega(\gamma_i-\gamma_j)^2$ which reduces the level of competition between phenotypes as the phenotypes become more dissimilar. When ω is sufficiently small in the asymmetric case, one of the sub-populations eventually goes extinct.

A well-known example of this is finches, where birds with different beak sizes feed on different size seeds. Finches with similar beak sizes experience a higher level of competition with similar phenotypes than with finches that have dissimilar beak sizes (Grant and Grant 2006). See Pelletier et al. (2009), Schoener (2011) for more examples where eco-evolutionary modelling has been studied.

Our aim is to create a much simpler population model that reproduces the phenotype equations (1) behaviour and is amenable to analysis that can provide insights into the reasons for the behaviours. We first consider a single population model in the "Modelling framework and a heuristic model" section, and then introduce a two sub-population model in the "A two sub-population simulation model" section. The distributions produced by the phenotype model, which solved 100 coupled ordinary differential equations, will be used to validate the results of an equivalent six-equation two sub-population model.

Modelling framework and a heuristic model

The six-equation model presented in the "A two sub-population simulation model" section is the appropriate simulation model to compare evolutionary branching

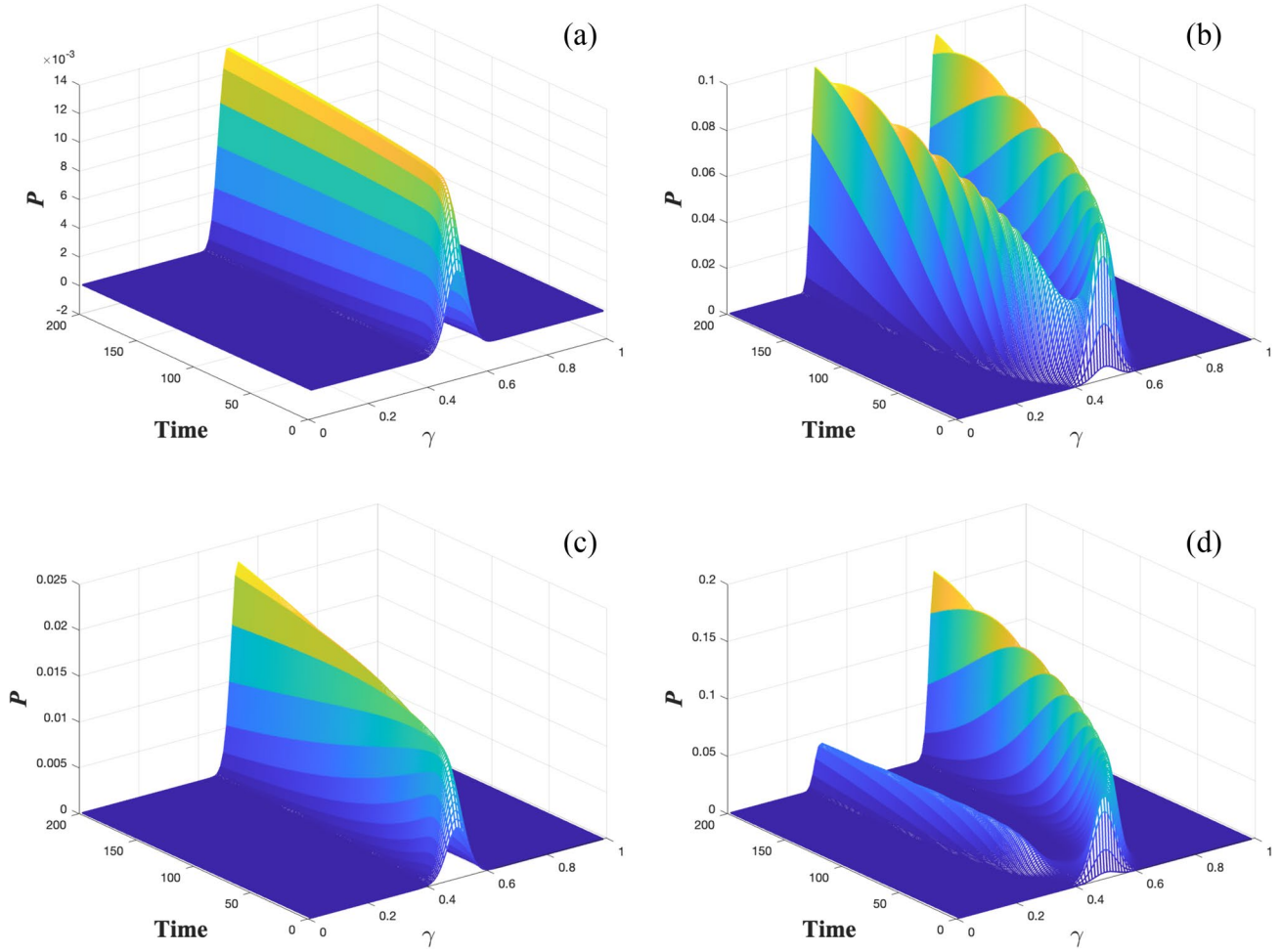

Fig. 1 Distributions of phenotype abundances produced by the phenotype model (1) for varying values of density-independent mortality (σ) and fitness landscape asymmetry (γ_C): **a** $\sigma = 2.00$, $\gamma_C = 0.500$; **b** $\sigma = 0.50$, $\gamma_C = 0.500$; **c** $\sigma = 2.00$, $\gamma_C = 0.40$; **d** $\sigma = 0.50$, $\gamma_C = 0.40$. Other parameter values used were $\mu = 10$; $\kappa = 0.10$; $\rho = 4.00$; $\eta = 0.50$; and $\omega = 6$. Initial conditions were $\sum P_i = 0.050$ with phenotype abundances distributed according to a beta distribution with shape parameters $\alpha = 100 = \beta$. A population of 100 phenotypes was used for these simulations

behaviour with the phenotype model (1), but this model is sufficiently high dimensional that analysis of its basic properties is not straightforward. Hence, we first present a simple model, approximately equivalent to (1), that may be analysed more readily in order to understand the sorts of behaviours that we might expect from the more complex model.

In the cases where the phenotype model does not show evolutionary branching (Fig. 1a, c) the simple model is able to reproduce the single population predictions of the phenotype model very accurately. However, in cases where branching does occur (Fig. 1b, d) the simple model can be used to predict the potential for such branching, but is unable to simulate such branching.

The simple three-equation single population eco-evolutionary model provides a fitness landscape that can be viewed explicitly in three dimensions. We apply a single delta function phenotype to the phenotype model (1) to define a corresponding fitness function for a single population model with analogous properties to the phenotype model (1). The delta function considers the average trait value of the population, $\hat{\gamma}$, and has values $P_i = P$ at $\gamma_i = \hat{\gamma}$ and $P_i = 0$ for all $\gamma_i \neq \hat{\gamma}$. This identifies a population P with the phenotype mean trait value $\hat{\gamma}$ and a fitness function $\hat{f}(\hat{\gamma};P)$. This model is developed in order to gain insight into the dynamical properties that underlie the branching behaviours observed in Fig. 1.

Eco-evolutionary population modelling framework

The canonical equations of the eco-evolutionary framework used here, for a population P that grows or reduces

in accordance with how it interacts with its environment and other populations, described by the population fitness function $\hat{f}$, with an evolving mean trait value $\hat{\gamma}$, and a trait differentiation Q (Cropp and Norbury 2022), are:

$$\begin{aligned}\frac{dP}{dt} &= P\left(\hat{f} + \frac{1}{2}\hat{\gamma}(1-\hat{\gamma})Q\frac{\partial^2\hat{f}}{\partial\hat{\gamma}^2}\right),\\ \frac{d\hat{\gamma}}{dt} &= \hat{\gamma}(1-\hat{\gamma})Q\frac{\partial\hat{f}}{\partial\hat{\gamma}},\\ \frac{dQ}{dt} &= Q^2\left((1-2\hat{\gamma})\frac{\partial\hat{f}}{\partial\hat{\gamma}} + \hat{\gamma}(1-\hat{\gamma})\frac{\partial^2\hat{f}}{\partial\hat{\gamma}^2}\right),\end{aligned} \tag{2}$$

where subscripts denoting multiple populations with many, one or no evolving traits, have been omitted for clarity (see Appendix "Extended eco-evolutionary population modelling framework" section for a fully annotated two-population modelling framework). The net per capita phenotype growth function averaged (in the small variance limit) over the phenotype distribution, $\hat{f}$, may be considered a measure of population fitness. The first derivative $\partial\hat{f}/\partial\hat{\gamma}$ in equation (2) is often referred to as a fitness or selection gradient, that determines the direction of adaptation. The second derivative $\partial^2\hat{f}/\partial\hat{\gamma}^2$ is the curvature of the fitness landscape which narrows or widens the distribution of phenotype abundances, and when negative is associated with evolutionary stability.

This framework assumes that the distribution of the population phenotype abundances over the trait γ, on the scaled trait interval $0 < \gamma < 1$, may be described by a beta distribution with a mean value $\hat{\gamma}$ and variance v. The state variable Q describes the trait differentiation of the population. The variance of the distribution is calculated using $v = \hat{\gamma}(1-\hat{\gamma})Q$. The derivation of these equations is provided in Cropp and Norbury (2022) using a moment-based method; an alternative derivation based on an asymptotic boundary layer analysis is provided in Appendix "Asymptotic derivation" section. Note that in the phenotype model of the "A phenotype model with evolutionary branching" section, v is directly calculated from the phenotype distribution.

Equations (2) form a single eco-evolutionary population modelling framework that is the basis for modelling many evolutionary scenarios. This modelling framework assumes no sources of additional phenotypic diversity such as the immigration of mutants from outside the evolutionary space. Phenotype diversity is incorporated through the initial conditions, and is modified by the population dynamics and selection pressures. The framework can accommodate ecosystems with many populations, each of which may have no, one, or many traits that evolve, and can represent stabilising, directional, and disruptive selection.

A particular eco-evolutionary system is defined by specifying an $\hat{f}$ for each population, which provides a $\frac{dP}{dt}$ equation. The $\hat{f}$ may include none, one, or several evolving traits, where each evolving trait mean has corresponding equations for $\hat{\gamma}$ and Q. That is, a $\frac{d\hat{\gamma}}{dt}$ and a $\frac{dQ}{dt}$ equation are obtained for each evolving trait using the $\hat{f}$. One or more populations may be considered sub-populations, or phenotype groups, of a population if their $\hat{f}$ have the same form and differ only in the names of the evolving parameters.

A simple analogy of the phenotype model

The population fitness function corresponding to that of the phenotype model (1), for a single population P feeding on a limiting recycling resource N with a mean trait value of $\hat{\gamma}$ is:

$$\hat{f} = \frac{\mu\hat{\gamma}(1-\hat{\gamma})N}{(N+\kappa)} - \frac{P}{\eta + \rho(\hat{\gamma}-\hat{\gamma}_C)^2} - \sigma. \tag{3}$$

Resource recycling is imposed by a conservation condition $N = 1 - P$. Differentiating this condition produces an equation for dN/dt that describes the recycling process. When the limiting resource is a nutrient, recycling implies remineralisation of organic material into inorganic nutrient N.

The terms in (3) are explained in (1). Note that the $\omega(\gamma_i - \gamma_j)^2$ term of the phenotype model (1), which captures competition between phenotypes, cannot be represented in this simple population model (3). This model is presented to help understand the properties of the two-sub-population model. The two-sub-population model presented in the "A two-sub-population simulation model" section is the appropriate model to compare simulation results with the phenotype model.

The fitness function (3) is inserted into the single population, single evolving trait eco-evolutionary modelling framework (2) (Appendix "Extended eco-evolutionary population modelling framework" section, Cropp and Norbury (2022)), to give the eco-evolutionary model:

$$\begin{aligned}\frac{dP}{dt} &= P\left(\begin{array}{c}\frac{\mu\hat{\gamma}(1-\hat{\gamma})N}{(N+\kappa)} - \frac{P}{\eta+\rho(\hat{\gamma}-\hat{\gamma}_C)^2} - \sigma +\\ \frac{1}{2}\hat{\gamma}(1-\hat{\gamma})Q\left[-\frac{2\mu N}{N+\kappa} + \frac{2\rho(\eta-3\rho(\hat{\gamma}-\hat{\gamma}_C)^2)P}{(\eta+\rho(\hat{\gamma}-\hat{\gamma}_C)^2)^3}\right]\end{array}\right),\\ \frac{d\hat{\gamma}}{dt} &= \hat{\gamma}(1-\hat{\gamma})Q\left(\frac{\mu(1-2\hat{\gamma})N}{(N+\kappa)} + \frac{2\rho(\hat{\gamma}-\hat{\gamma}_C)P}{(\eta+\rho(\hat{\gamma}-\hat{\gamma}_C)^2)^2}\right),\\ \frac{dQ}{dt} &= Q^2\left(\begin{array}{c}(1-2\hat{\gamma})\left[\frac{\mu(1-2\hat{\gamma})N}{(N+\kappa)} + \frac{2\rho(\hat{\gamma}-\hat{\gamma}_C)P}{(\eta+\rho(\hat{\gamma}-\hat{\gamma}_C)^2)^2}\right] +\\ \hat{\gamma}(1-\hat{\gamma})\left[-\frac{2\mu N}{N+\kappa} + \frac{2\rho(\eta-3\rho(\hat{\gamma}-\hat{\gamma}_C)^2)P}{(\eta+\rho(\hat{\gamma}-\hat{\gamma}_C)^2)^3}\right]\end{array}\right).\end{aligned} \tag{4}$$

The resource is recycled and its mass (of limiting nutrient) is conserved in this simple scaled system, so that $N = 1 - P$, and a differential equation to describe changes in N is not necessary.

We evolve the trait mean $\hat{\gamma}$ and the trait differentiation Q so that the trait variance is given by $v(t) = \hat{\gamma}(t)(1-\hat{\gamma}(t))Q(t)$. Note that this model simulates the process in the phenotype

model (1) where phenotypes with trait values near γ_C, equivalent to $\hat{\gamma}_C$ in (4), endure greater negative effects of competition than phenotypes with trait values further from γ_C.

The fitness landscape

The fitness landscape for this model is a surface in three-dimensional $(P, \hat{\gamma}, \hat{f})$ space, similar to those of Hui et al. (2021), that does not depend on Q. The $(P, \hat{\gamma}, Q)$ solution space for (4) is a three-dimensional phase space that includes Q, but as Q is generally small and always positive, the phase space may be examined in a representative two-dimensional section for a specific value of Q. The details of the $(P, \hat{\gamma})$ phase plane (Fig. 3) change a little with different values of Q but not sufficiently to warrant drawing separate phase planes.

The internal eco-evolutionary equilibrium points of the framework equations (2), where $P \neq 0$ and $\hat{\gamma} \neq 0, 1$, ignoring the Q, including the three internal eco-evolutionary equilibrium points of the simple model (4) (Fig. 2), have the properties, if we take Q small and positive, that:

$$\begin{aligned} &\hat{f}_P \approx 0, \qquad \frac{\partial \hat{f}_P}{\partial \hat{\gamma}} = 0, \\ &\lambda_1 \approx \frac{\partial \hat{f}_P}{\partial P} P, \ \lambda_2 = \hat{\gamma}(1-\hat{\gamma}) Q \frac{\partial^2 \hat{f}_P}{\partial \hat{\gamma}^2}. \end{aligned} \tag{5}$$

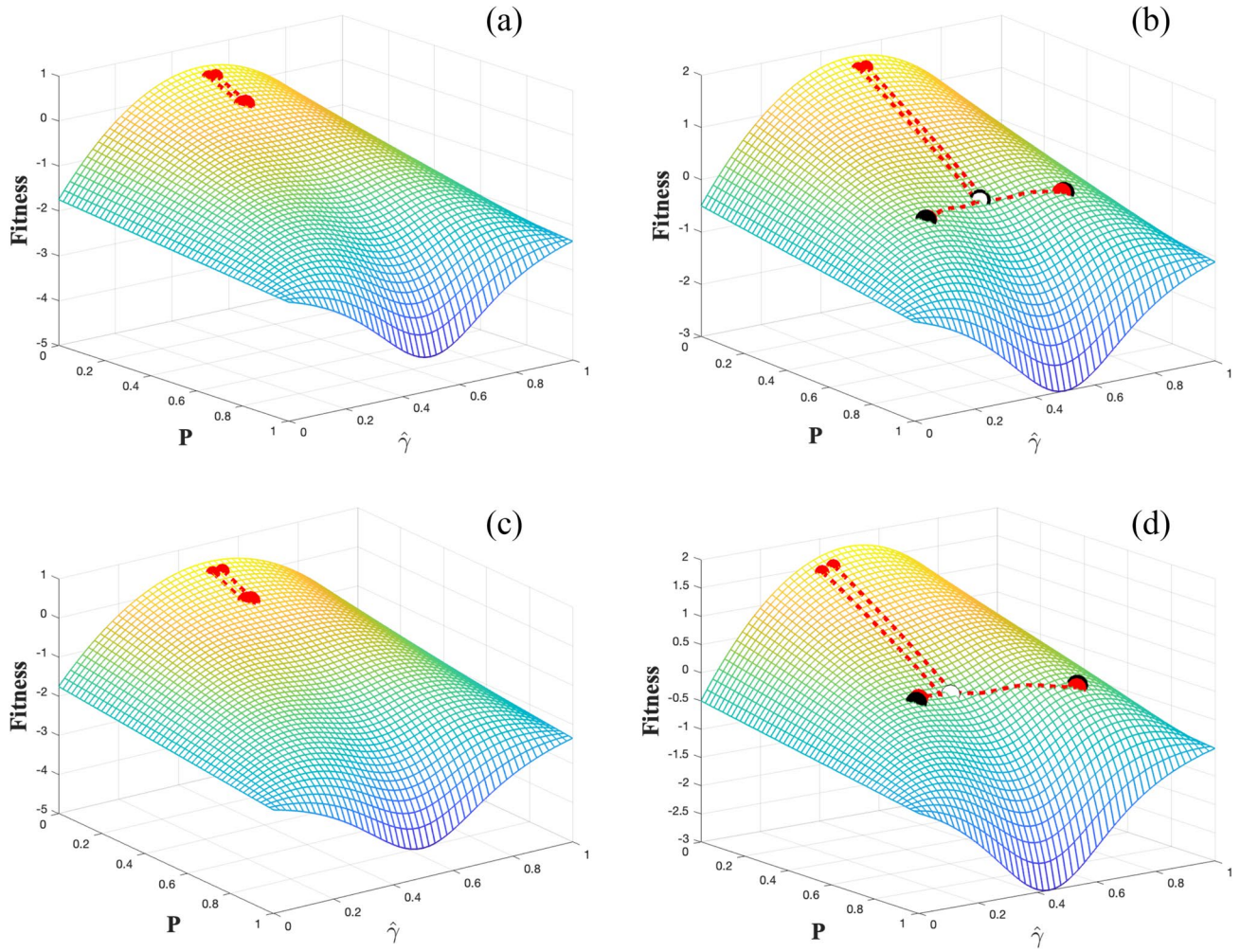

Fig. 2 Fitness landscapes for the simple model (3) for **a** the symmetric case ($\hat{\gamma}_C = 0.50$) with high mortality ($\sigma = 1.75$); **b** the symmetric case with low mortality ($\sigma = 0.50$); **c** an asymmetric case ($\hat{\gamma}_C = 0.40$) with high mortality ($\sigma = 1.75$); and **d** an asymmetric case ($\hat{\gamma}_C = 0.40$) with low mortality ($\sigma = 0.50$). Other parameter values as for the phenotype model simulations shown in Fig. 1. Stable eco-evolutionary equilibrium points are shown by black dots and unstable points by white dots. The black dots in (**a**) and (**c**) are obscured by the red dots showing the final state of the system, but are evident in panels (**b**) and (**d**). Two separate integration trajectories are shown by the dashed red lines. The symmetric cases (**a** and **b**) have one trajectory starting from $\{P = 0.05, \hat{\gamma} = 0.475, Q = 0.005\}$ and one from $\{P = 0.05, \hat{\gamma} = 0.525, Q = 0.005\}$. The asymmetric cases (**c** and **d**) have one starting from $\{P = 0.05, \hat{\gamma} = 0.360, Q = 0.005\}$ and one from $\{P = 0.05, \hat{\gamma} = 0.410, Q = 0.005\}$. Note the centre of the valley between the two ridges is located at $\hat{\gamma} = 0.50$ in the symmetric case (**a**), and at $\hat{\gamma} \approx 0.40$ in the asymmetric case (**b**)

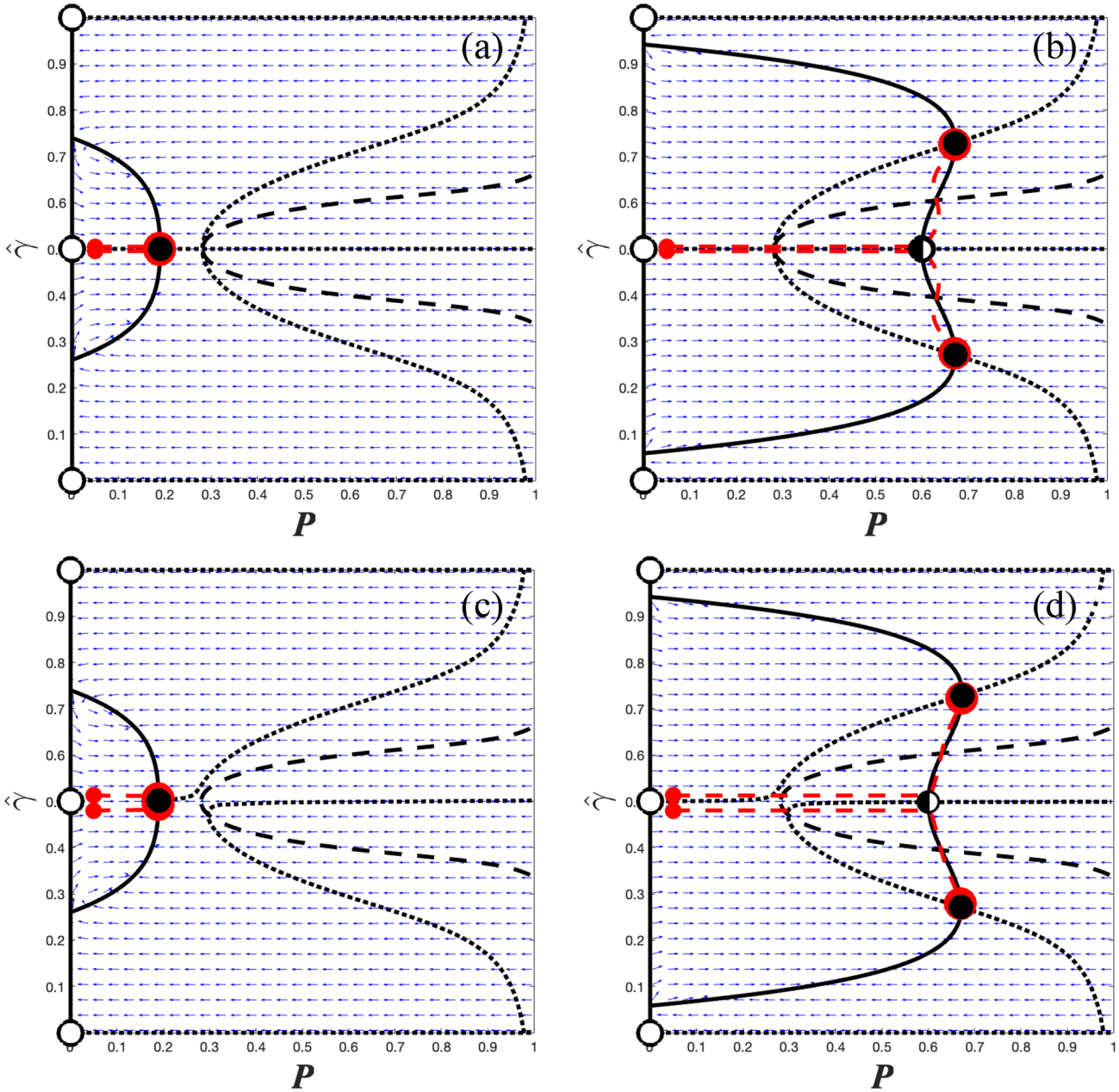

Fig. 3 Phase planes and vector fields for the single population model (4). Mortality (σ) values are **a** 1.75; **b** 0.50; **c** 1.75; and **d** 0.50. Cases and parameter values as for Fig. 2 except that $\hat{\gamma}_C$ is increased from 0.40 to 0.499 for the two asymmetric cases to show the symmetry breaking. The solid black lines in the phase plane are the $P = 0$ and $\hat{f} = 0$ isoclines. The dotted lines are the $\hat{\gamma} = 0$, $\hat{\gamma} = 1$, and $\partial\hat{f}/\partial\hat{\gamma} = 0$ isoclines. Panels (**a**) and (**b**) also have $\hat{\gamma} = 0.5$ isoclines. Unstable equilibrium points are shown by white dots, and stable ones by black dots; the latter are overlaid in the diagrams by the large red dots showing the final states of the integrations. The saddle point appears as a half-white, half-black dot in the phase plane. The dashed line shows the zero curvature isocline where $\partial^2\hat{f}/\partial\hat{\gamma}^2 = 0$. Two integration trajectories are shown by the dashed red lines. Trajectories as for Fig. 2

The first pair of properties (the intersections of the zero isoclines) determines the location of each point, and the signs of the second pair (the eigenvalues of each internal equilibrium point) determine their stability. The approximations are the result of ignoring small variance terms.

Figure 2 illustrates how the changing density-independent mortality σ affects the solutions. The fitness landscape of the system simply translates with the change in σ; the key change that affects the outcome of the model is that the system is restricted to low values of P when σ is large. This

restricts the system to the region of the fitness landscape where the curvature in the $\hat{\gamma}$ dimension is negative (i.e. concave), stabilising the equilibrium point as the gradient in the P direction is always negative. Reducing σ allows the system to occupy the valley region of the fitness landscape where the $\hat{\gamma}$ curvature is positive (i.e. convex), which directs the system to one of the stable equilibrium points that appear on the ridges.

Figure 2 reveals that the fitness landscape of this single population system changes significantly as the population increases. Intra-population competition is low when the population is small, and the system has a fitness landscape with negative curvature in the $\hat{\gamma}$ dimension that indicates stabilising selection and no potential for evolutionary branching. As the population increases the intra-population competition also increases and causes the fitness landscape to buckle, with a valley and two ridges becoming obvious from around $P \approx 0.5$. A stable eco-evolutionary equilibrium point is located on each of these ridges, revealing that the single population system has two distinct stable equilibrium points, with the outcome of any integration determined by the initial conditions.

Located within the valley lies an unstable eco-evolutionary equilibrium point, with attributes $\frac{\partial \hat{f}}{\partial P} < 0$ and $\frac{\partial^2 \hat{f}}{\partial \hat{\gamma}^2} > 0$, similar to some requisites for evolutionary branching (Geritz et al. 1997, 1998). The quantities that determine the stability of the point are the eigenvalues of the Jacobian matrix of the system evaluated at the point (5). These are related to the gradient and curvature of the fitness surface, and ensure that the point has an attracting eigenvector in the P direction and a repelling eigenvector in the $\hat{\gamma}$ direction, that is, this point is an unstable saddle point. This positive second trait derivative causes this point to be unstable in the $\hat{\gamma}$ direction. The attracting eigenvector lies along the $\hat{\gamma} = 0.50$ line in the symmetric case, and nearby in the asymmetric case (i.e. between the two red dashed lines in panels (a and c) and (b and d) of Fig. 2 respectively). In each case, the attracting eigenvector forms a separatrix that divides the system into two parts, and determines which of the two stable equilibrium points the system will be attracted to.

Dynamical properties

The properties of the internal eco-evolutionary equilibrium points are confirmed by the trajectories of two integrations of the system shown in Figs. 2 and 3. The integrations start from initial conditions on either side of the separatrix, are initially attracted to the (unstable) saddle equilibrium point, but are then repelled from this point to end at the stable equilibrium point on the appropriate ridge shown in Fig. 2b, d and the zero isocline intersection in Fig. 3b, d.

It is interesting to note that although changing the value of the population mortality σ only subtly alters the shape of the fitness landscape, it can significantly alter the region of the fitness landscape that the system explores. When the population has low mortality rates (Fig. 2b, d), the system explores a region of the fitness landscape where it has the potential for evolutionary branching. As the mortality rate increases, the population eventually loses this potential (Fig. 2a, c), providing theoretical evidence of the potential for environmental change to affect the fundamental properties of ecosystems.

Figure 3 shows that a bifurcation occurs in the system's eco-evolutionary solution space as σ is reduced. When $\sigma^* \approx 1.490$ the symmetric case undergoes a pitchfork bifurcation, when the previously stable equilibrium point becomes unstable, and two stable branches are created, one either side of the original point (Fig. 3b). This process creates an unstable saddle point that is key to evolutionary branching. The effect of this saddle point on trajectories starting on either side of the separatrix is evident in Fig. 3. Rather than the trajectories converging as they did for large σ (panel a), the saddle point now causes them to ultimately diverge and be attracted to different stable equilibrium points.

The zero curvature ($\partial^2 \hat{f} / \partial \hat{\gamma}^2 = 0$) isocline shown as the dashed black line in Fig. 3 provides information on the dynamics of the evolutionary branching. The sign of the curvature determines the sign of the key eigenvalue that controls the stability of the internal equilibrium points (5). The trajectories in Fig. 3b to the left of the zero curvature isocline are slowly converging, as the curvature is small and negative. When the trajectories cross the dashed black line the curvature becomes small and positive, and the trajectories begin to move apart. We call this behaviour, which occurs in the region of the fitness landscape between the dashed line and the branching point in Fig. 3b and d, "weakly branching" as $\hat{\gamma}$ changes very slowly in this region. When the trajectories arrive at the branching point, they are in a region where the fitness landscape is more strongly positively curved, and the trajectories diverge more rapidly. However, each trajectory soon moves into a region where the curvature is strongly negatively curved, and they are attracted to their respective stable equilibria.

The branching dynamics predicted by the properties of the fitness landscape and the solution space of the symmetric case of the simple model (Figs. 2b and 3b) agree with those observed for the symmetric case of the phenotype model in Fig. 1b. In both instances, the population splits smoothly and symmetrically into two equivalent-sized sub-populations that have mean trait values equally distant from $\hat{\gamma}_C$.

The bifurcation in the asymmetric case occurs slightly differently. The bifurcation still occurs at approximately the same value of σ^* but now the stable equilibrium point

moves upward in the $\hat{\gamma}$ dimension and an unstable and stable pair of points appear below it in an imperfect pitchfork (or apparently blue-sky) bifurcation, ultimately producing an outcome and eco-evolutionary branching properties similar to the symmetric case. The different forms of bifurcation indicated by the simple model are evident in the distributions produced by the phenotype model, as differences in the branching process.

However, multiple numerical simulations of the phenotype model (1) reveal that the bifurcation value of σ of the phenotype model is different from that of the single population model. This is likely due to the absence of any representation of the $\omega(\gamma_i - \gamma_j)^2$ term in the simple model. Nonetheless, the correspondence between the behaviour of the phenotype model (Fig. 1) and the properties of the single population model predicated by its fitness landscapes and vector fields (Figs. 2 and 3) suggest that the single model provides useful insights into certain behaviours of the phenotype model. For example, it may predict the existence and types of bifurcations but not their specific locations.

Figure 3b and d suggests the existence of two distinct zones of eco-evolutionary behaviour that underpin the AD approach (Dieckmann and Law 1996): an "ecological" zone that extends from the initial condition to the trajectory approaching the saddle point; and an AD zone between the saddle point and the stable equilibrium points.

The system transitions from its initial ecological behaviour (between the initial condition and the dashed line where $\partial^2\hat{f}/\partial\hat{\gamma}^2 = 0$) to weakly branching in the zone between the dashed line and the saddle point, where $\partial^2\hat{f}/\partial\hat{\gamma}^2 > 0$ (recall (5)) — we refer to this as the non-equilibrium dynamics (NED) zone. The system then transitions to strongly branching behaviour in the AD zone, which occurs after the trajectories leave the immediate neighbourhood of the saddle point. The NED zone will be discussed further in the "The non-equilibrium dynamics zone" section in the Appendix.

The single population model predicts and reproduces the results of the phenotype model well for $\sigma = 2$ when no evolutionary branching occurs (Fig. 1a and c), but cannot reproduce the evolutionary branching evident in Fig. 1b and d. We next produce an extended model with two sub-populations to do this.

A two-sub-population simulation model

To reproduce the evolutionary branching evident in our phenotype model we consider an equivalent eco-evolutionary population model with two sub-populations of sizes P_1 and P_2. Hence, we apply two delta functions simultaneously, at trait values $\gamma = \hat{\gamma}_1, \hat{\gamma}_2$ respectively, to the phenotype model (1) to produce fitness functions $\hat{f}_1$ and $\hat{f}_2$ for two sub-populations that represent two groups of phenotypes. We obtain the fitness functions, $\hat{f}_1$ and $\hat{f}_2$, that each has the same form and parameter values as they are drawn from the same initial population, but each has its own trait mean, $\hat{\gamma}_1$ and $\hat{\gamma}_2$.

The fitness functions:

$$\hat{f}_i = \frac{\mu\hat{\gamma}_i(1-\hat{\gamma}_i)N}{(N+\kappa)} - \frac{P_i}{\eta + \rho(\hat{\gamma}_i - \hat{\gamma}_C)^2} - \frac{P_j}{\eta + \rho(\hat{\gamma}_i - \hat{\gamma}_C)^2 + \omega(\hat{\gamma}_i - \hat{\gamma}_j)^2} - \sigma, \quad (6)$$

here for $i,j = 1,2$, $(i \neq j)$, are included in the population framework (34), for two populations where each independently evolves its own trait mean and differentiation. See (1) for ecological definitions of the terms and parameters in equation (6). We now create our eco-evolutionary two-sub-population model that will be compared to the phenotype model (1):

$$\begin{aligned}
\frac{dP_i}{dt} &= P_i\left(\hat{f}_i + \frac{1}{2}\hat{\gamma}_i(1-\hat{\gamma}_i)Q_i\frac{\partial^2\hat{f}_i}{\partial\hat{\gamma}_i^2} + \frac{1}{2}\hat{\gamma}_j(1-\hat{\gamma}_j)Q_j\frac{\partial^2\hat{f}_i}{\partial\hat{\gamma}_j^2}\right),\\
\frac{d\hat{\gamma}_i}{dt} &= \hat{\gamma}_i(1-\hat{\gamma}_i)Q_i\frac{\partial\hat{f}_i}{\partial\hat{\gamma}_i},\\
\frac{dQ_i}{dt} &= Q_i^2\left((1-2\hat{\gamma}_i)\frac{\partial\hat{f}_i}{\partial\hat{\gamma}_i} + \hat{\gamma}_i(1-\hat{\gamma}_i)\frac{\partial^2\hat{f}_i}{\partial\hat{\gamma}_i^2}\right),
\end{aligned} \quad (7)$$

where:

$$\begin{aligned}
\frac{\partial\hat{f}_i}{\partial\hat{\gamma}_i} &= \frac{\mu(1-2\hat{\gamma}_i)N}{N+\kappa} + \frac{2\rho(\hat{\gamma}_i - \hat{\gamma}_C)P_i}{(\eta + \rho(\hat{\gamma}_i - \hat{\gamma}_C)^2)^2} + \frac{2[\rho(\hat{\gamma}_i - \hat{\gamma}_C) + \omega(\hat{\gamma}_i - \hat{\gamma}_j)]P_j}{(\eta + \rho(\hat{\gamma}_i - \hat{\gamma}_C)^2 + \omega(\hat{\gamma}_i - \hat{\gamma}_j)^2)^2},\\
\frac{\partial^2\hat{f}_i}{\partial\hat{\gamma}_i^2} &= -\frac{2\mu N}{N+\kappa} - \frac{8\rho^2(\hat{\gamma}_i - \hat{\gamma}_C)^2P_i}{(\eta + \rho(\hat{\gamma}_i - \hat{\gamma}_C)^2)^3} + \frac{2\rho P_i}{(\eta + \rho(\hat{\gamma}_i - \hat{\gamma}_C)^2)^2}\\
&\quad + \frac{2(\rho+\omega)P_j}{(\eta + \rho(\hat{\gamma}_i - \hat{\gamma}_C)^2 + \omega(\hat{\gamma}_i - \hat{\gamma}_j)^2)^2} - \frac{8[\rho(\hat{\gamma}_i - \hat{\gamma}_C) + \omega(\hat{\gamma}_i - \hat{\gamma}_j)]^2P_j}{(\eta + \rho(\hat{\gamma}_i - \hat{\gamma}_C)^2 + \omega(\hat{\gamma}_i - \hat{\gamma}_j)^2)^3},\\
\frac{\partial^2\hat{f}_i}{\partial\hat{\gamma}_j^2} &= \frac{8\omega[\rho(\hat{\gamma}_i - \hat{\gamma}_C) + \omega(\hat{\gamma}_i - \hat{\gamma}_j)](\hat{\gamma}_i - \hat{\gamma}_j)P_j}{(\eta + \rho(\hat{\gamma}_i - \hat{\gamma}_C)^2 + \omega(\hat{\gamma}_i - \hat{\gamma}_j)^2)^3}\\
&\quad - \frac{2\omega P_j}{(\eta + \rho(\hat{\gamma}_i - \hat{\gamma}_C)^2 + \omega(\hat{\gamma}_i - \hat{\gamma}_j)^2)^2}.
\end{aligned} \quad (8)$$

Now $N = 1 - \sum_i P_i$. We evolve the sub-population measures P_1 and P_2, with their trait means $\hat{\gamma}_1$ and $\hat{\gamma}_2$, and their trait differentiations Q_1 and Q_2, after stating suitable parameters and initial conditions.

This eco-evolutionary population model simulates two sub-populations P_1 and P_2, that together form a population P that consumes a resource N in order to grow. The net growth rate of each sub-population P_1 or P_2 represents competition for the resource N, and a trade-off of its growth against the cost of evolving defences against intra-specific competition. This trade-off is captured by the trait means $0 < \hat{\gamma}_1, \hat{\gamma}_2 < 1$. The population maximises its growth rate when $\hat{\gamma}_1$ or $\hat{\gamma}_2$ equals $\frac{1}{2}$, but suffers its maximum density dependent mortality, from intra-specific competition, when $\hat{\gamma}_1$ or $\hat{\gamma}_2$ equals $\hat{\gamma}_C$.

The model has a six-dimensional phase space $\{P_1, P_2, \hat{\gamma}_1, \hat{\gamma}_2, Q_1, Q_2\}$, and a hypersurface for each fitness landscape

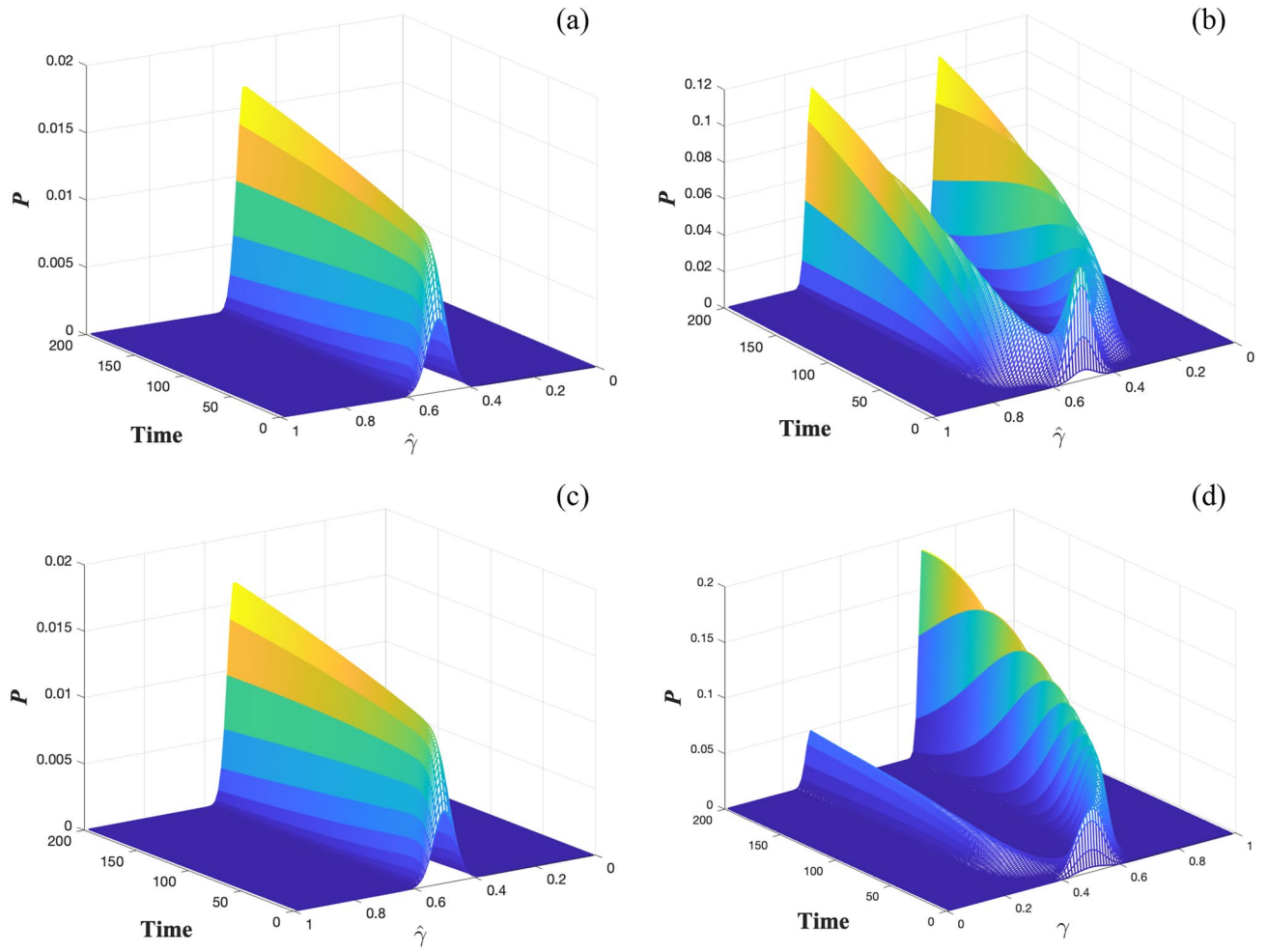

Fig. 4 Distributions of phenotypes (assuming beta distributions) produced by the two-sub-population model (6)–(8) for simulations using the same parameter values and initial conditions as those shown in Fig. 1 for the phenotype model (1). Note these results reproduce the essence of the results of the phenotype model (1) shown in Fig. 1, including the different forms of evolutionary branching in the symmetric and asymmetric cases

in five-dimensional space $\{P_1, P_2, \hat{\gamma}_1, \hat{\gamma}_2, \hat{f}_1 \text{ or } \hat{f}_2\}$, as Q_1 and Q_2 are not involved in the population fitness terms. The properties of the system are complicated to analyse and difficult to visualise even in three dimensions. However, when $\hat{\gamma}_1 \approx \hat{\gamma}_2$, which is the situation which usually precedes evolutionary branching, we can reduce the dimension of the model if we take $P_1 \approx P_2$ and $Q_1 \approx Q_2$, so that $\hat{f}_1 \approx \hat{f}_2$. Then Figs. 2 and 3 provide a starting point to understanding the more complicated model.

The details of the numerical simulations of this model are provided in Appendix "Numerical simulations" section. We use these numerical simulations to construct Figs. 4 to 8 in the manuscript and Figs. 9 to 15 in the Appendix. The phenotype distributions in Fig. 4 were created by estimating the beta distribution shape parameters at each generation from the trait means and variances (from $v_i = \hat{\gamma}_i(1-\hat{\gamma}_i)Q_i$) and using these to construct beta distributions for each population of each generation as described in Appendix "Numerical simulations" section.

Results and discussion

Phenotype distributions produced by the two sub-population model (6)–(8) (Fig. 4) are very similar to those produced by the phenotype model (1) (Fig. 1). These simulations used the same parameter values and similar initial conditions, and provided an initial validation of the two-sub-population model.

The distributions produced by the two-sub-population model agrees qualitatively with those of the phenotype model in that larger values of density-independent mortality σ suppress evolutionary branching, and that symmetric

and asymmetric fitness landscapes produce different forms of evolutionary branching. Further, the model results for the sub-population biomasses, the trait means, and the trait variances at the end of the integration agree quantitatively. A detailed examination of the correspondence between the end states of the solutions of the phenotype and population models shown in Figs. 1 and 4 is provided in Appendix "Final distributions" section.

The agreement between the preliminary results of these models suggests that a detailed examination of the dynamical properties of the population model (7), (8) may provide useful insights into the dynamics of the equivalent phenotype model. Further, both model results agree broadly with the bifurcation properties of the single population model (Fig. 3) with the exception of the critical value of σ that defines the bifurcation point. This will be considered further in the "Bifurcation behaviours" section, where it is shown that the two-sub-population model successfully predicts the bifurcation value.

Equilibrium states

The evolutionary branching behaviours of the two-sub-population model evident in Fig. 4b and d are further examined by considering two-dimensional ecological and trait sections of the six-dimensional phase space (Fig. 5). The four solution trajectories shown in these figures each start from different initial values of the trait means. These initial conditions were chosen to demonstrate that all stable equilibria in the state spaces may be accessed.

When this system has a symmetric fitness landscape ($\hat{\gamma}_C = 0.50$, a and b) the ecology has a single stable equilibrium point and the traits have two stable equilibrium points separated by a separatrix that links five unstable equilibria. All trajectories finish at the same ecological equilibrium but may finish at different trait equilibriums. The symmetric fitness case with $\sigma < \sigma_*$ appears to have only eco-evolutionary branching solutions, as there are no other stable equilibrium points in the interior or on the boundaries of the evolutionary (trait) space.

The introduction of asymmetry into the fitness landscape ($\hat{\gamma}_C = 0.40$, Fig. 5c and d) introduces a third stable equilibrium point into the evolutionary space, and allows for solutions that do not involve evolutionary branching. For the chosen parameter values, this solution is only available to trajectories that commence with large trait means, and then only to a small cohort of initial conditions that are attracted to the stable equilibrium point and not the nearby unstable saddle that initiates branching for large trait means.

The asymmetric case also has slightly different equilibrium states in the ecological space. Each stable equilibrium in the evolutionary space is associated with a slightly different stable equilibrium location in the ecological space. The stable ecological equilibrium for the $\hat{\gamma}_1 \approx 0.7, \hat{\gamma}_2 \approx 0.3$ evolutionary equilibrium point is shown as the black dot in Fig. 5c; the equilibrium points for the other trajectories lie at the large red dot at their termination. Nearby equilibria in the ecological space can have very different evolutionary outcomes associated with them.

An interesting attribute of many of the ecological trajectories shown in Fig. 5a and c is that many initial conditions lead to "evolutionary rescue" (Bell 2017). Systems that start with sub-populations that have similar mean trait values (as all evolutionary branching scenarios do) have $\hat{f}_i = 0$ isoclines in the ecological space that are nearly parallel. In these cases, small changes in mean trait values can move the stable ecological equilibrium point where both sub-populations coexist dramatically, pushing this point through the boundary creating a stable single sub-population equilibrium on the boundary through a trans-critical bifurcation. Eventually, the coexistence point can go to infinity and back, creating a stable equilibrium point on the opposite boundary where the other sub-population dominates. Further changes can then cause the unstable coexistence equilibrium point to re-enter the state space through the opposite boundary and create a new stable coexistence point within the state space through a second trans-critical bifurcation. These behaviours suggest evolutionary rescue may be a common feature of such systems, as is evidenced by the trajectories in Fig. 5a and c that almost intersect the P_2 axis, suggesting that at one time in the integration the $P_1 = 0$ equilibrium points were stable.

Note that the details of the diagrams in Fig. 5 are slightly different for the other initial conditions as the trajectories finish in different regions of the six-dimensional space. Hence equilibrium points may appear to lie in different locations. As the vector fields are drawn for the final state of the simulation, but the trajectories are for the whole integration, separatrices may appear to be crossed in these figures.

The simple model (4) showed that breaking the fitness landscape symmetry (i.e. $\hat{\gamma}_C \neq 0.5$) leads to different forms of bifurcation behaviour when σ is varied. We now explore the behaviour of the two sub-population model for symmetric and asymmetric cases.

Bifurcation behaviours

The bifurcation behaviour of a dynamical system is a fundamental property of the system and may be used to compare the attributes of different models or different modelling approaches. The vector fields of the simple system (4) in Fig. 3 reveal that the model with a symmetric fitness landscape (a and b) bifurcates slightly differently from the same model with an asymmetric fitness landscape (c and d). Although bifurcations also occur in the ecological space (see Figs. 10–12 in Appendix "Bifurcation

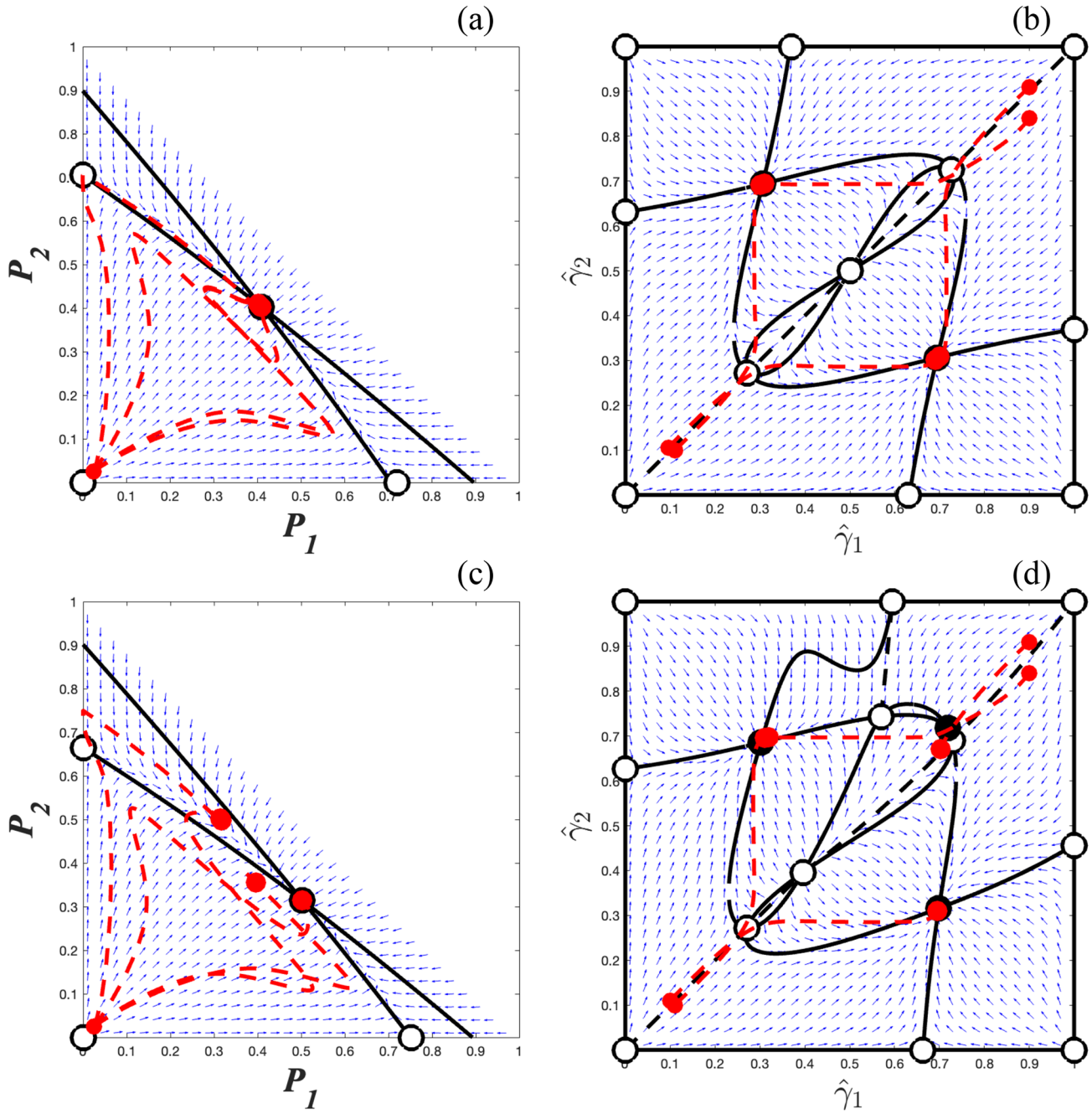

Fig. 5 Vector fields produced by the two-sub-population model based on (6)-(8) for a symmetric fitness landscape ($\hat{\gamma}_C = 0.50$, **a** and **b**), and an asymmetric fitness landscape ($\hat{\gamma}_C = 0.40$, **c** and **d**). Other parameter values used as for Fig. 4. Four trajectories from four different $\hat{\gamma}_1$ and $\hat{\gamma}_2$ initial conditions are plotted in each vector field: 1) $\hat{\gamma}_1 = 0.0950$, $\hat{\gamma}_2 = 0.1050$,; 2) $\hat{\gamma}_1 = 0.0110$, $\hat{\gamma}_2 = 0.1000$; 3) $\hat{\gamma}_1 = 0.9000$, $\hat{\gamma}_2 = 0.9100$; and 4) $\hat{\gamma}_1 = 0.9000$, $\hat{\gamma}_2 = 0.8400$. Other initial values are $P_1 = 0.0250 = P_2$, $Q_1 = 0.0050 = Q_2$. The zero isoclines, equilibrium points, and vector fields are drawn at the final state of the first set of initial conditions, so do not necessarily agree with the other trajectories. Note the evolutionary rescue in (**a**) and (**c**) where one trajectory in each diagram almost intercepts the P_2 axis

dynamics" section), here we focus on bifurcations in the evolutionary space.

The simple model predicts that the symmetric case will undergo a pitchfork bifurcation to create the evolutionary branching point and that the asymmetric case will undergo an imperfect pitchfork, or blue sky, bifurcation. The difference in the way the branching points are created produces a detectable difference in the way branching occurs in the model simulations. A smooth, symmetric branching of the initial population into two equal sub-populations is predicted

by the simple model for the symmetric case (Fig. 3b). This dynamic is evident in the plots of the phenotype distributions of both the phenotype and two sub-population models (Figs. 1b and 4b).

The asymmetric case of the simple model predicts that evolutionary branching in this case will occur differently from the symmetric case. Instead of a smooth splitting into two sub-populations, it predicts that the initial population will change its mean trait value and grow before a second sub-population appears with a different mean trait value and commences to grow (Fig. 3d). This branching dynamic is again evident in the plots of the phenotype distributions of both the phenotype and two sub-population models (Figs. 1d and 4d).

The qualitative differences in how evolutionary branching occurs in the symmetric and asymmetric cases of the phenotype and two-sub-population model evident in Figs. 1 and 4 are predicted by the simple model. The properties of the saddle points that form the evolutionary branching points are the same in the symmetric and asymmetric cases, but the bifurcations by which the points are created differ. These differences lead to differences in the dynamics of how the populations branch. That the simple model (4) is able to predict what is observed in the phenotype model, and that the two-sub-population model (6)-(8) is able to reproduce the dynamics, are compelling evidence that the eco-evolutionary modelling framework (2) is able to capture key properties of these systems.

While the single population model is useful in understanding how and why the evolutionary branching behaviours in the phenotype model are different as a result of introducing asymmetry into the fitness landscape, its simplicity prevents it from identifying specifics such as the critical value of the bifurcation parameter σ. The single population model predicts that the bifurcations occur at significantly different σ^* values to those predicted by numerical experiments for the phenotype model and the two-sub-population model. However, the latter values are very similar, with both the phenotype model and the two-sub-population model bifurcating at $\sigma^* = 1.75$.

The transition from a single-population solution to a two-population solution occurs when the $\hat{f} = 0$ isocline, shown in Fig. 3 as a solid line, passes through the $\partial\hat{f}/\partial\hat{\gamma} = 0$ isocline, shown in Fig. 3 as a dotted line, from left to right. This coincides with a change in sign of the curvature (approximately in the asymmetric case) as the $\partial^2\hat{f}/\partial\hat{\gamma}^2 = 0$ isocline, shown in Fig. 3 as a dashed line, is tangential with the $\partial\hat{f}/\partial\hat{\gamma} = 0$ isocline in the centre of the eco-evolutionary space in the symmetric case, and nearly tangential in the asymmetric case. This bifurcation point, where $\partial\hat{f}/\partial\hat{\gamma} = 0$ and $\partial^2\hat{f}/\partial\hat{\gamma}^2 = 0$, is most simply explored by taking the density-independent mortality σ as the bifurcation parameter (see Fig. 3).

For the case $\hat{\gamma}_C = 0.5$ ($\hat{f}_i$ symmetry in evolutionary space) when $\hat{\gamma}^* = \hat{\gamma}_1^* = \hat{\gamma}_2^* = \hat{\gamma}_C$, we use $\hat{f}_i\big|_{\hat{\gamma}_i^*=0.5} = 0$ to calculate the bifurcation point:

$$\sigma^* = \frac{\mu}{4}\frac{N^*}{N^*+\kappa} - \frac{1-N^*}{\eta}. \tag{9}$$

We find $N^* = 1 - P_1^* - P_2^* = 1 - 2P_1^* = 1 - P^*$ as the symmetric case has $P_1^* = P_2^*$, using the zero curvature condition:

$$\frac{N^*}{N^*+\kappa} = \left(\frac{\rho}{\eta^2} + \frac{\omega}{2\eta^2}\right)(1-N^*). \tag{10}$$

Using this N^* in (9) gives $\sigma^* = 1.75$ in the symmetric case, which agrees with the phenotype model calculation to two decimal places. When $\hat{\gamma}_C \neq 0.5$ (asymmetric $\hat{f}_i$ in evolutionary space) the bifurcation is imperfect, and the isocline equation $\{\partial\hat{f}_i/\partial\hat{\gamma}_i = 0\}$ is now used to find $\hat{\gamma}_i^*$.

Some key stages in the bifurcation behaviour of the two-sub-population model with a symmetric fitness landscape are shown in Fig. 6. For all $\sigma > \sigma^* = 1.75$ the evolutionary section of the vector field looks like panel (a), with a single stable equilibrium point in the phase space and no possibility of evolutionary branching. Reducing σ to 1.50 (panel b) introduces a supercritical pitchfork bifurcation into the previously stable equilibrium producing two stable equilibrium points separated by a saddle point. This initiates evolutionary branching in the model. As σ further reduces (panel c) the stable equilibria move apart and the zero isoclines through the saddle extend until the saddle splits into an unstable node with two saddle points (panel d). This arrangement (as shown in Fig. 5b) remains relatively unchanged in the symmetric fitness case as σ reduces further.

A similar presentation of the bifurcation properties of the asymmetric case of the eco-evolutionary model (6)-(8) is provided in Appendix "Bifurcation dynamics" section. Further, a comparison of Fig. 6c, d hints that further bifurcations may be possible, but would require a model with more sub-populations to explore.

Eco-evolutionary dynamics and *Q*

Time series of the first 100 generations of the simulations of the evolutionary branching solutions of the eco-evolutionary population model shown in Fig. 4b and d are provided in Fig. 7. In both the symmetric (Fig. 7a) and asymmetric (Fig. 7b) cases the evolutionary branching processes are accompanied by significant increases in Q, and hence the variance, of the sub-populations. In the symmetric case, both sub-populations simultaneously increase Q by about 50% as their distributions spread symmetrically as phenotypes with better trade-offs between growth and competition out-grow the initially

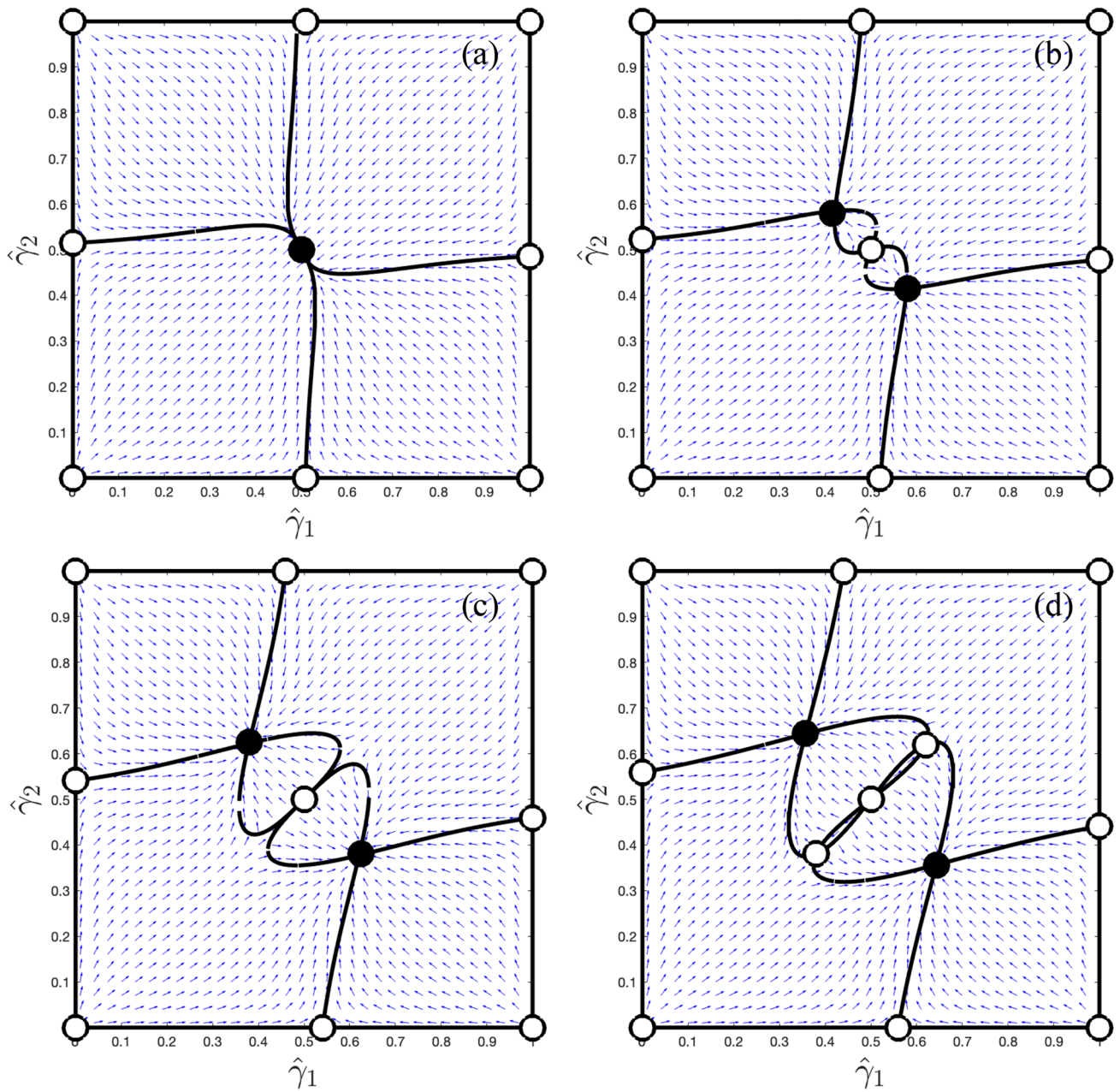

Fig. 6 The evolutionary space ($\hat{\gamma}_1$ - $\hat{\gamma}_2$) vector fields produced by the two-sub-population model based on (6) for a symmetric fitness landscape ($\hat{\gamma}_C = 0.50$) with: **a** $\sigma = 1.75$ (the bifurcation value); **b** $\sigma = 1.50$; **c** $\sigma = 1.20$; and **d** $\sigma = 1.00$. Other parameter values used as for Fig. 4

most abundant phenotypes. The Q values then reduce as the two sub-populations establish coexistence at stable equilibriums with different mean trait values. Note that the peaks in Q coincide with rapid changes in the trait means.

The branching process occurs differently in the asymmetric case. Here, the Q_1 value for the P_1 population (panel (b), red line) increases by about an order of magnitude during the evolutionary branching process while the Q_2 value of the P_2 sub-population (panel (b), blue line) does not change. This is consistent with P_2 following the stable branch in the vector field (Fig. 3d) while the P_1 sub-population "jumps" to the stable equilibrium point created by the imperfect, or blue sky, bifurcation.

The increase in Q_1 facilitates an increase in the variance of the P_1 phenotype distribution as phenotypes in the vicinity of the second mean trait equilibrium, that started with small initial abundances, increase in abundance, and result in P_2's mean trait value $\hat{\gamma}_2$ increasing. This soon establishes a second sub-population mode, with intermediate phenotype abundances reducing to near zero to create sub-populations with different trait modes.

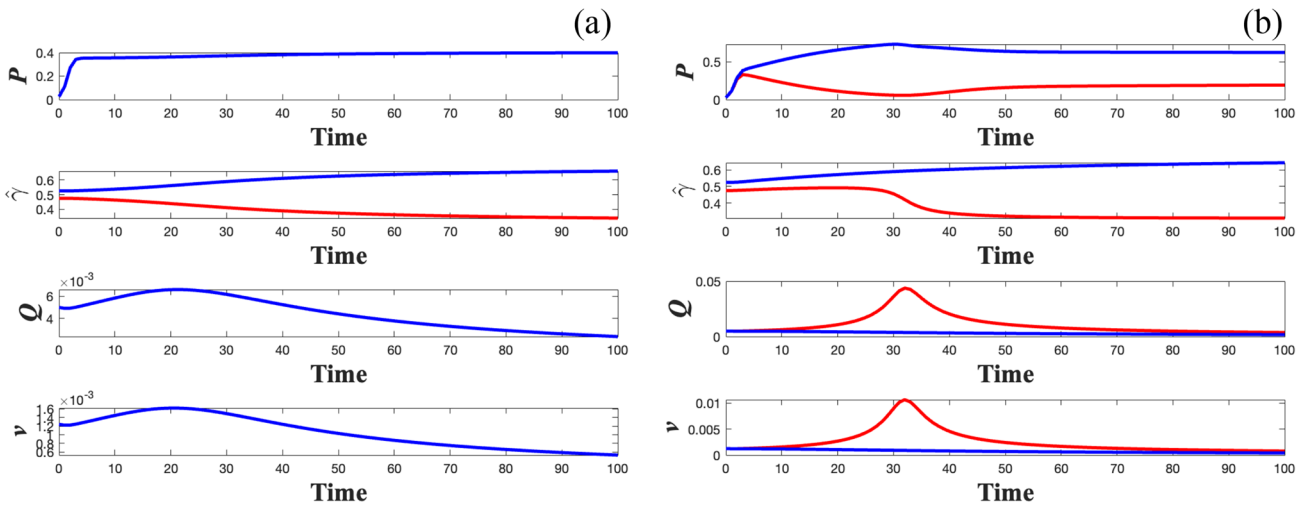

Fig. 7 The time series of state variables for the first 100 generations of the integrations of the eco-evolutionary population model (6)-(8) shown in: **a** Fig. 4b; and **b** Fig. 4d. The time series shown are the population size in each of the sub-populations (P, top), the average phenotype value for each sub-population ($\hat{\gamma}$, second panel), the trait differentiation (Q, third panel), and the trait variance of each sub-population (v, bottom). Time series data for P_1 is shown by the red line and P_2 by the blue line in each case. These are overlaid for P, Q, and v in (**a**). Note the correspondence of the peaks in Q and v with changes in the average phenotype value

These time series reveal the importance of Q in evolutionary branching, as increases in the Qs allow the variances of the sub-populations to increase as the sub-populations sample the evolutionary space for better options. This is consistent with an increase in variance that is considered a condition for evolutionary branching (Wakano and Iwasa 2013).

Note that although Fig. 7 shows the sub-population sizes and trait means have stabilised by about 100, and the Qs and variances are near zero, Fig. 4 shows that the dynamics of the system are not completely over. This is a further advantage of simulating Q in these systems, as although the cross-sectional areas and the locations of the distributions of the sub-populations in evolutionary space in the population model have stabilised by about time step 100, the shapes of the distributions have not. Even though the Qs and vs are very small, the variances of the distributions in Fig. 4 continue to decrease. This agrees with the results of the phenotype model shown in Fig. 1.

Sectioning the phase space

The six-dimensional solution space of the two-sub-population model presents difficulties in visualising the properties of the system, and in Figs. 5 and 6, we examined sections through the space. This presents a problem analogous to Plato's Allegory of the Cave: how do we understand the true properties of the system from the snippets that we can visualise?

We now consider in some detail the eco-evolutionary dynamics of the two-sub-population model (6), (34) with an asymmetric fitness landscape to assess the usefulness of various sections through the solution spaces of these models. Two-dimensional ecological, evolutionary, and eco-evolutionary sections through the six-dimensional phase space of this model are shown as vector fields in Fig. 8.

In contrast to the eco-evolutionary space of the single population model (Fig. 3) which showed the entire solution space (apart from small changes associated with changes in Q), the eco-evolutionary sections through the six-dimensional solution space of the two sub-population model (Fig. 8a and b) are harder to interpret for the mechanics of evolutionary branching. The eco-evolutionary sections $(P_i, \hat{\gamma}_i)$ have only one stable equilibrium point each, although they suggest that other instantiations of the model may have more than one. The arrangements of the zero isoclines also suggest that the only bifurcations that will occur in the vicinity of the solutions shown are transcritical bifurcations that occur when either of the sub-populations goes extinct. The important bifurcations that facilitate evolutionary branching in this model are captured solely in the evolutionary section.

The ecological (c) and evolutionary (d) sections through the solution space, however, provide very useful descriptions of the system, and clearly show a stable ecological equilibrium state accompanied by a stable evolutionary equilibrium state that is one of three stable evolutionary equilibria available to the system. The trajectory through the ecological space suggests that more complex dynamics than are implied by the final zero isoclines and vector field have occurred during the simulation. The two reversals of the direction of the trajectory demonstrate the potential for evolutionary rescues to occur as stable equilibria leave and enter the

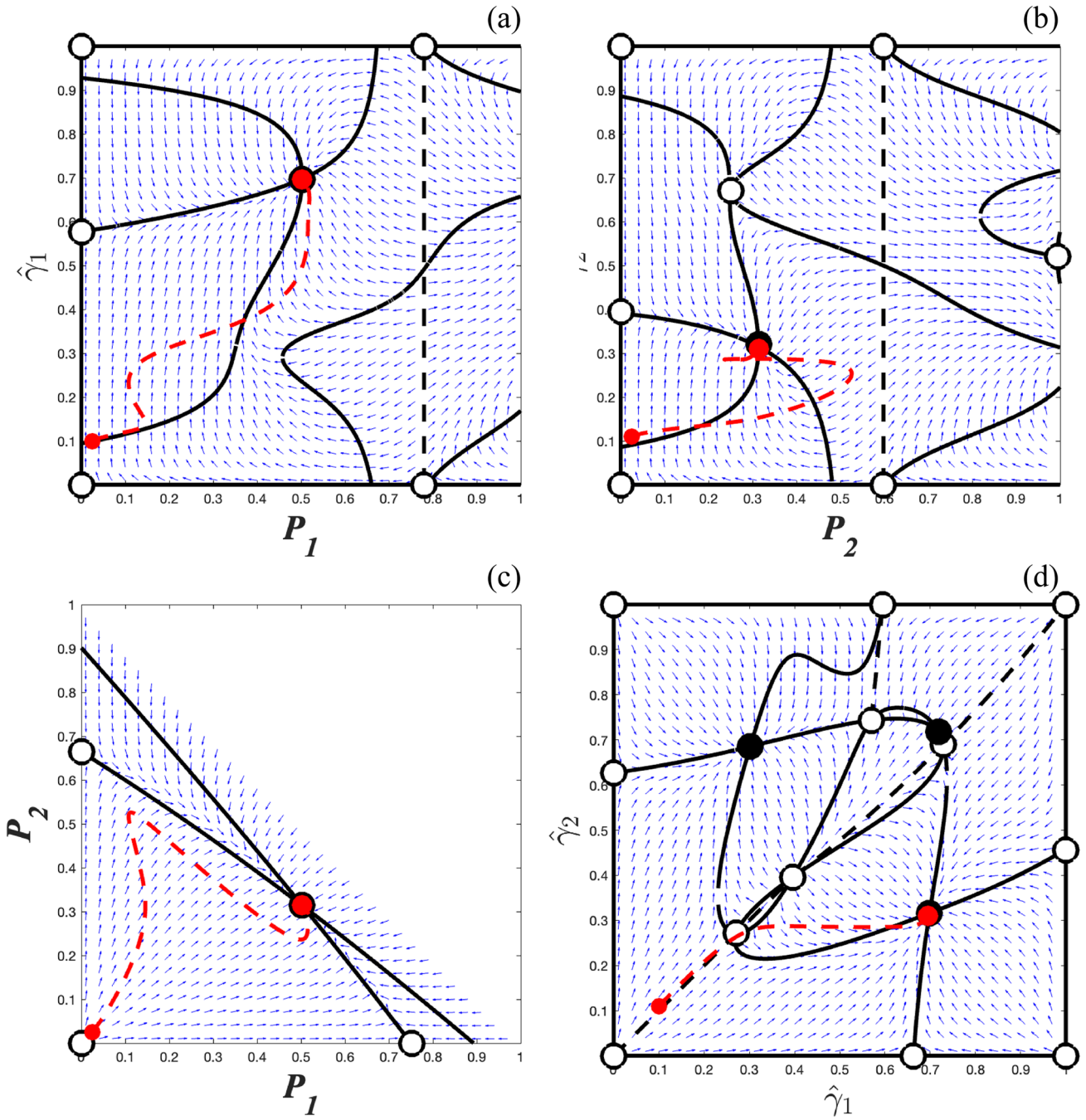

Fig. 8 End-of-integration phase plane sections from the eco-evolutionary population model (6)-(8). Phase plane details as for Fig. 7 except that trait mean initial conditions were changed to $\hat{\gamma}_1 = 0.1000, \hat{\gamma}_2 = 0.1100$. The integration was extended to time 1,000 for the phase plane diagrams to ensure the system reached eco-evolutionary equilibrium. Separatrices are shown as dashed black lines but are not apparent where coincident with zero isoclines. The trajectories may cross separatrices in these diagrams as the trajectories are for the whole integration and the location of the separatrices is shown only for the end of the integration

ecological state space through transcritical bifurcations on the boundary (see Figs. 10 to 12 in Appendix "Bifurcation dynamics" section).

Whether evolutionary rescue occurs in a particular simulation depends upon the choice of parameters and initial conditions. For some choices, one population can become extinct. Generally, simulations that seek to reproduce evolutionary branching are initiated with two very similar subpopulations. This similarity means that their ecological zero isoclines are nearly coincident so that subtle changes

in mean trait values can lead to dramatic changes in the location and stability of ecological equilibrium points. This can result in the ecology being attracted to one boundary equilibrium point, then an opposite one, before being attracted to a stable interior equilibrium, as shown in Fig. 8c. This suggests that the potential for evolutionary rescue is a common attribute of these systems.

Further, the ecological isoclines in Fig. 8c show that the system has evolved to a state that reduces the effect of evolutionary changes on the ecological state. This is evidenced by the zero isoclines becoming less parallel, indicating that the system has formed two relatively robust sub-populations with different trait means. Note that the property of nearly coincident zero isoclines does not apply to the evolutionary space so trajectories through the evolutionary space are generally simple, with the system initially being attracted to a saddle point which then directs the system to an evolutionary branching solution with $\hat{\gamma}_1 \neq \hat{\gamma}_2$.

We have considered here only a simple model of a population that undergoes evolutionary branching. More complex scenarios with more populations and more evolving traits increase the dimensionality of the solution spaces we seek to understand, but we remain restricted to visualising two-dimensional sections. Visualising a sequence of such sections at multiple points of a solution, as is presented in Appendix "Bifurcation dynamics" section, is arduous but provides further insights into the properties of the solution space. Developing a solid understanding of simple systems such as (4), whose fitness landscapes and solution spaces can be visualised (almost) in their entirety, may be the best aid to inform interpretations of the properties of more complex systems.

Conclusions

This work has demonstrated the validity of the eco-evolutionary modelling framework (2), and its extension to multiple populations (34). The framework assumes that population fitness functions mirror individual growth functions, that phenotype abundances have beta distributions across traits, and that the trait differentiation Q is fundamental to simulating key evolutionary processes such as branching. This confirms previous testing of this framework in other evolutionary scenarios (Cropp and Norbury 2021, 2022).

The correspondence between the predictions of a model of trait evolution that simulates the dynamics of each phenotype, without assuming a particular distribution of traits or a fitness function, and those of our eco-evolutionary population model suggests the modelling framework captures the essence of evolutionary change. This correspondence is evident both in simple comparisons of the changes over time of the phenotype abundances and in comparisons of fundamental properties of the systems such as bifurcation behaviours. The simulations confirm the efficacy of small variance approaches to the modelling of evolution in populations. While this work assumed beta-distributed traits, closely related results have been obtained by oligomorphic approaches that assumed normal distributions (Lion et al. 2023).

The differences in bifurcation behaviour inferred from the simple population model (4) in this work, that indicated the bifurcation from a non-branching solution to a branching solution would occur as a symmetric pitchfork bifurcation in a symmetric fitness landscape but as an imperfect pitchfork (or blue-sky) bifurcation in an asymmetric fitness landscape appear to be borne out by the dynamics of the phenotype model (1). Despite the simple model being only an approximation to the full model (6)-(8), the correspondence between the dynamics of the branching of the phenotype model (Fig. 1) and the full model (Fig. 4) suggest that the three models exhibit the same fundamental properties. In particular, the differences in the branching dynamics between the symmetric and asymmetric cases in the models demonstrate that all three models have pitchfork bifurcations in the symmetric fitness landscape and imperfect pitchfork/blue sky bifurcations in the asymmetric fitness landscape.

In the context that the results presented in this work support the equivalence of the phenotype and population modelling approaches, and the utility of the simple population model in understanding the properties of both the more complicated models, we make the following observations:

- the eco-evolutionary modelling framework (2), within which specific models are obtained by defining an $\hat{f}_i$ and $\hat{\gamma}_i$(s) for each population P_i, can provide plausible simulations of evolutionary processes;
- generic properties of the modelling framework and simple versions of complex models can provide insights into the dynamical properties induced by coupled eco-evolutionary feedbacks in more complex eco-evolutionary systems;
- the heuristic model provides a theoretical basis for an argument that environmental change could affect the manner in which an ecosystem adapts, in particular, whether it is capable of evolutionary branching or not;
- changes in the variance of the phenotype distribution predicted by Q appear to be important in evolutionary branching, as it allows the variance in the system to spike, but remain bounded (Figs. 7b and 15);
- evolutionary branching produces a two sub-population system with an equilibrium state that becomes less sensitive to evolutionary feedback as it evolves;
- systems may have multiple eco-evolutionary stable states, that may simultaneously represent single or branched

populations, with which equilibrium is found in a simulation depending on the initial conditions;
- using asymmetric initial conditions on symmetric phase planes may break the symmetry of solutions over early evolutionary time scales. Ultimately, symmetry such that $\hat{\gamma}_2^* = 1 - \hat{\gamma}_1^*$ (Fig. 14c) is restored as the system approaches eco-evolutionary equilibrium.

We note that in simulations of evolutionary branching, because the two sub-populations are drawn from the same population, the sub-population initial conditions are nearly identical, and their zero isoclines are nearly coincident in the ecological space until evolution creates two distinct sub-populations. This creates a sensitive system, in which small changes (evolutionary or environmental) can dramatically change the location of stable equilibrium points. As the sub-populations evolve their zero isoclines rotate and intersect in a more robust and stable ecological equilibrium point. These properties may facilitate sequential "evolutionary rescues" of the sub-populations while their trait means slowly change, but leave feasible that sub-populations that may coexist in a stable environment do not co-exist in a variable environment.

Further, when simulating real systems such as those influenced by climate change, that perforce include environmental forcings, eco-evolutionary stable equilibria in simulations move in response to external forcings, and evolutionary outcomes may become contingent upon the environment (Wong 2019). Although not examined in this work, the potential for equilibrium points to be moved through bifurcations that create or destroy evolutionary branching points is particularly interesting. The adaptation of marine phytoplankton, with their rapid reproduction rates and strong seasonal dynamics, to warming oceans may be an interesting example of this problem. This may be especially pressing given the role of marine phytoplankton in maintaining the level of carbon dioxide and oxygen in the atmosphere (Irwin et al. 2015; Padfield et al. 2017; Hinners et al. 2017; Ward et al. 2019; Le Gland et al. 2021; Beaufort et al. 2022; Behrenfeld et al. 2022) and mediating the transfer of climatically important gases between the ocean and atmosphere (Charlson et al. 1987; Lancelot et al. 2010; Bullock et al. 2017).

Eco-evolutionary modelling and the commonly used AD method, applied to the same dP/dt and $d\hat{\gamma}/dt$ equations, produce the same equilibrium solutions for an arbitrary small positive value of Q. Dynamically simulating Q is the major difference between our eco-evolutionary modelling framework and AD, and this is important in being able to simulate the dynamics of evolving ecosystems. In particular, Fig. 7 demonstrates that increasing variance is a key aspect of evolutionary branching. Further, AD is predicated on the ecological system having a stable equilibrium state located within the feasible region of the ecological state space. Eco-evolutionary dynamics have no such constraint, and our simulations show that significant evolutionary change can occur in systems when the ecological equilibrium state lies outside the feasible region of the ecological state space. Our eco-evolutionary modelling framework extends AD from long-term equilibrium solutions to much more of the dynamical system solution space.

The development of population-level eco-evolutionary models such as those presented here greatly reduces the number of equations involved compared to phenotype models and facilitates the inclusion of eco-evolutionary processes in plankton ecosystems into global climate models. This work provides a specific example of where joint feedback between ecological and evolutionary dynamical processes have significant outcomes; here, evolutionary branching can depend on the dynamical path taken. Perhaps, the most significant outcome of this work is the general framework for modelling eco-evolutionary systems and the understanding it can facilitate into the mechanisms underlying the dynamics of eco-evolutionary systems in general, and evolutionary branching in particular.

Appendix

Phenotype distributions

Phenotype models generally make no assumptions about how the population is distributed among the phenotypes, but population models generally do (Lande 1976; Klauschies et al. 2018; Cropp and Norbury 2022). To support the assumptions that underpin the eco-evolutionary population modelling framework (Appendix "The population evolutionary framework"), we examine the distributions produced by the phenotype model (1).

Four simulations are shown in Fig. 9, each with the same parameter set but with different distributions of the population among the phenotypes for initial conditions. These simulations show that even non-smooth initial distributions can produce smooth final distributions that are beta-distributed.

We tested the distributions produced by the phenotype model (1) for similarity to a beta distribution using the two-sample Kolmogorov-Smirnoff test (Stephens 1974; Naaman 2021). The results of these tests (Table 1) indicate that the phenotype model maintains beta distributions when initiated with a beta distribution, and produces phenotype distributions that are not significantly different from beta distributions from a variety of non-beta initial distributions.

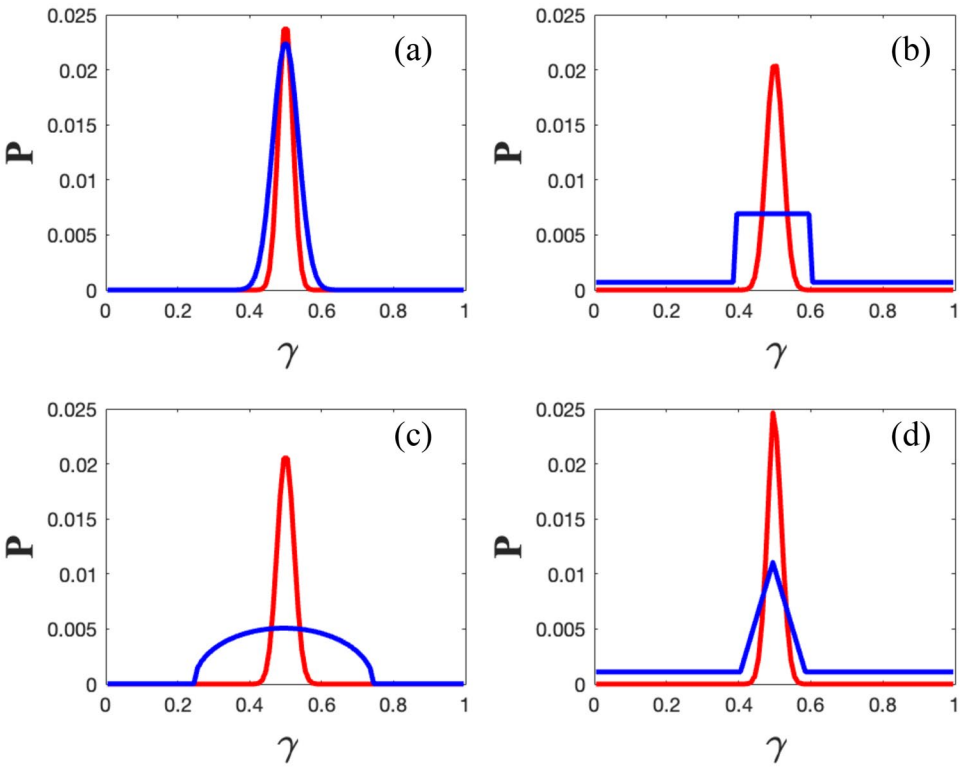

Fig. 9 Initial (blue lines) and final (red lines) distributions of the phenotype model (1) for initial conditions: **a** beta; **b** square; **c** semi-circular; and **d** triangular distributions. The model was integrated for 100 generations with 100 phenotypes using the parameter values $\mu = 10$; $\kappa = 0.10$; $\rho = 4.00$; $\eta = 0.50$; $\omega = 6$, $\sigma = 2.00$, $\hat{\gamma}_C = 0.50$. As shown in Fig. 1 the large values of σ result in single peaked distributions

The eco-evolutionary framework

The eco-evolutionary framework comprises ecological and evolutionary axioms that together provide a robust template for modelling how the properties of populations change over long evolutionary time scales. The ecological axioms have been previously set out in detail in Cropp and Norbury (2015) so only a brief summary is provided here.

The ecological framework

The ecological equations are written in a currency of a limiting nutrient, that is each population x_i is measured in terms of its share of the total (finite, constant) amount of limiting nutrient cycling in the ecosystem at any time $t > 0$. The canonical form of the ecological population equations for m interacting populations is:

$$\frac{dx_i}{dt} = x_i f_i(\Omega; N, x_1, x_2, \ldots, x_m), \text{ for } i = 1, 2, \ldots, m, \tag{11}$$

where Ω is the set of parameters that control interactions between populations, and their environment, $N = N_T - x_1 - x_2 - \cdots - x_m$ is the fraction of the total limiting nutrient cycling in the system in the abiotic nutrient pool. $N_T > 0$ is the initial total limiting nutrient in the system, typically scaled so that $N_T = 1$, and $x_1, x_2, \ldots, x_m$ are the m living population shares of the limiting nutrient. Here, each f_i represents the x_i population's interactions with the other populations and their environment. The f_i usually have positive (feeding, mutualism) and negative (competition, mortality) terms. Throughout, each f_i is a smooth function of all its variables (and, later, its evolutionary parameters) so that Taylor series expansions always exist. Equation (11) has a unique positive solution for the positive initial data $0 < x_1(0), x_2(0), \ldots, x_m(0), N(0)$ and $x_1(0) + x_2(0) + \cdots + x_m(0) + N(0) = N_T$.

The ecological modelling approach we use Cropp and Norbury (2015) implements basic criteria on the f_i that realistic ecosystem models should satisfy:

– each population grows (dies) according to the constraints imposed by the other populations and the

Table 1 Results of two-factor Kolmogorov-Smirnoff tests comparing final distributions of the simulations in Fig. 9 against beta distributions with the same mean and variance

Figure 9 case	Initial distribution	Final distribution	p	Test statistic
(a)	Beta	Beta	0.9921	0.0600
(b)	Square	Beta	0.6766	0.1000
(c)	Semicircular	Beta	0.6766	0.1000
(d)	Triangular	Beta	0.1400	0.1600

environment, the latter represented here in its simplest form by the non-living nutrient pool N, independently of how we measure the populations and the scale of the ecosystem - this ensures population equations of the form (11). We use abundances which means that the total amount of limiting nutrient N_T in the populations and the nonliving nutrient pool is scaled to be one (100%);
- the total amount of limiting nutrient $N_T = 1$ is conserved as it moves through the food web so that $N(t) = 1 - \Sigma x_i(t)$ for all $t > 0$. Note $\frac{dN}{dt} = -\Sigma x_i f_i$ defines the dynamics of the nutrient pool;
- a predator cannot gain more nutrient than its prey loses, and any nonliving organic nutrient produced by the system, through senescence, mortality, or predation inefficiencies, is recycled into the inorganic nutrient pool. We assume that there is zero net immigration or emigration of every population (for the evolutionary aspect - more on this later), and that nutrient influx equals nutrient efflux (most delineated ecosystems recycle at least 90% of their limiting nutrient, see Loreau (2010); Vitousek and Matson (2012));
- the growth of every population is explicitly limited by the resources available to it - when its resources are maximal the population increases (i.e. it is viable), when its resources are zero, the population decreases (i.e. it is not immortal). That is, for any population x_i that utilises resource R_i for growth, $f_i|_{R_i=1} > 0 > f_i|_{R_i=0}$, where $R_i = N$ for autotrophs and $R_i = x_j,\ i \neq j$ for heterotrophs;
- the *per capita* growth rate of each population monotonically increases along resource rays that extend from point(s) of zero resource to point(s) of maximum resource;
- negative nutrient measures do not occur; that is, when the amount of nutrient in the abiotic resource pool is zero, it must strictly increase, that is $\frac{dN}{dt}\Big|_{N=0} > 0$, so that $N(t) > 0$ for all $t > 0$. Then $\Sigma x_i(0) < 1$ implies that $\Sigma x_i(t) < 1$ for all $t > 0$, which means that $x_i(t) < 1$ since $x_i(t) > 0$.

The last condition, which precludes negative values for the measures (shares) in ecologically realistic models, does not imply that we override any negative values that the system may produce, as is apparently done in some complex ecological simulation models. The condition in our models arises from the structure of the equations that define the model and is a property of the system. Populations that start with a positive share of the resource remain positive - that is $x_i(0) > 0$ implies that $x_i(t) > 0$ for all $t > 0$. When populations go extinct their share of the resource tends to zero.

The phenotype evolutionary framework

Evolution is the change in a heritable trait mean that is a characteristic of a population through time and over generations. Natural selection is the differential survival and reproduction of individuals due to differences in their phenotypes. Here, we model populations as made up of phenotypes defined by their trait parameter values, which are often scaled to lie in the unit interval. Random mutations in their genetic material passed on to offspring influence the heritable phenotypes.

The struggle for existence, in the context of other phenotypes, other populations, and the abiotic environment, leads to preferential survival of certain phenotypes (i.e. traits), and this defines the evolution of a population in terms of its changing trait mean. The distribution of traits in the population usually has a small variance, and this also evolves, tending to zero with stabilising selection in the absence of mutation. The total population, its trait mean, and trait variance are defined in (12):

$$\begin{aligned} P(t) &:= \int_0^1 P_\gamma(t)d\gamma, \quad \text{for } t \geq 0, \\ \hat{\gamma}(t) &:= \int_0^1 \gamma P_\gamma(t)d\gamma / P(t), \quad \text{for } t \geq 0, \\ v(t) &:= \int_0^1 (\gamma - \hat{\gamma}(t))^2 P_\gamma(t)d\gamma / P(t), \quad \text{for } t \geq 0. \end{aligned} \tag{12}$$

We aim to produce a simplified population model of evolution by taking a small variance asymptotic limit for the processes (captured in a phenotype equation) that define the struggle for existence amongst phenotypes, as defined by their common trait values. The processes that affect the abundances of phenotypes include interactions between phenotypes, both within and without the populations, interactions between phenotypes and their abiotic environment, and changes due to imperfect copying of genetic material during reproduction such as mutation and cross-over. The generic equation for the change in abundance of a phenotype P_γ is:

$$\frac{dP_\gamma}{dt} = P_\gamma f_P(\gamma; P_\xi) + \frac{\partial}{\partial \gamma}\left(m(\gamma, P_\gamma)\frac{\partial P_\gamma}{\partial \gamma}\right), \quad \text{for } t > 0,\ 0 < \gamma < 1. \tag{13}$$

Remember $f_P := f_P(\gamma; P_\xi) := f_P(\Omega, \gamma; P_\xi$ for $0 \leq \xi \leq 1)$ to make the notation less verbose.

Here, γ is the trait whose mean evolves, f_P is the *per capita* growth rate of the competing phenotypes, defined for each phenotype P_γ as it interacts with the other phenotypes P_ξ (for $\xi \neq \gamma$) and itself (for $\xi = \gamma$), and the diffusion-like term involving $m(\gamma, P_\gamma) > 0$ represents

mutation, imperfect copying, etc. The initial data $P_\gamma(0)$ is defined at $t = 0$ to be a beta distribution with mean $\hat{\gamma}(0)$ and small variance $v(0)$. We have no influx of phenotypes across the trait bounds $\gamma = 0$ and $\gamma = 1$, that is, we take no-flux boundary conditions at $\gamma = 0$ and $\gamma = 1$, so that the model does not include immigration or emigration of mutant phenotypes. Experimental evidence suggests that mutation rates are generally very small, in the order of 10^{-7}: in this paper, we take $m = 0$.

The evolutionary framework considers the evolution of a phenotype P_γ within a population P. The phenotype is identified by its value of the trait γ and its abundance is measured in the same framework as the ecological equations (11). The change in abundance of the phenotype is given by the canonical equation (13), where clonal reproduction only is considered in this paper, that is $m = 0$ in (13).

The evolutionary equations are subject to conditions that ensure that they reflect the principles of evolution by natural selection:

- the trait parameter that identifies each evolving phenotype P_γ is scaled so that it lies within the finite range $0 \le \gamma \le 1$ with no emigration/immigration at $\gamma = 0, 1$;
- the phenotypes P_γ within a population P are functionally equivalent, that is, each phenotype P_γ grows according to the same $f_P(\gamma;P_\xi)$, which defines membership of the population.

The population evolutionary framework

The population evolutionary framework is obtained by averaging over all the P_γ that together make up the population P:

- the average fitness of a population is modelled by its average growth function $\hat{f}_P(\hat{\gamma};P)$, that is, the $f_P(\gamma;P_\xi)$ evaluated at the population average trait value $\gamma = \hat{\gamma}$ for the total population P;
- system level traits, that capture the interaction between two populations and may appear in more than one population fitness $\hat{f}_P(\hat{\gamma};P)$, are influenced only by the fitness of their home population;
- the framework is always valid for populations with small trait variance and directional and stabilising selection ($\frac{\partial^2 \hat{f}_P}{\partial \hat{\gamma}^2} < 0$), and remains valid for destabilising selection when Q remains suitably bounded.

System-level traits may occur when traits are described in particular ways; for example, a predator-prey interaction may encapsulate the classic "arms race" in a single parameter that captures the predator's attack and the prey's defence. In such cases the predator and the prey may have traits that evolve to influence this interaction. These traits perforce appear in both the predator and the prey's $\hat{f}_P$. The final condition restricts the application of this evolutionary framework to non-disruptive selection.

Note that in the "The ecological framework" section, we restricted attention to f_P that have Taylor series expansions in all their arguments so that $\hat{f}_P$ inherits these smoothness properties in both $\hat{\gamma}$ and P. We can then either use the moment-based expansion (see Klauschies et al. (2018); Cropp and Norbury (2022)) or the asymptotic approximation (see the "Asymptotic derivation" section) to obtain the eco-evolutionary population modelling framework (2). This framework is closed with respect to the first three moments of the phenotype distribution, P, $\hat{\gamma}$, and v, which is valid on the evolutionary time scale proportional to the inverse of the trait differentiation, $1/Q$.

Asymptotic derivation

The cumulative distribution function (CDF) $\chi(t,\gamma)/P(t)$ for the probability density function (pdf) $P_\gamma(t)/P(t)$ satisfies the non-local hyperbolic partial differential equation:

$$\frac{\partial^2 \chi}{\partial t \partial \gamma} = \frac{\partial \chi}{\partial \gamma} f_P(\gamma; P_\xi), \tag{14}$$

in the strip $S = \{t, \gamma; 0 < t < \infty, 0 < \gamma < 1\}$, together with the initial and boundary conditions:

$$\chi(0,\gamma) = \chi_0(\gamma) := \int_0^\gamma P_{\tilde{\gamma}}(0) d\tilde{\gamma}, \quad 0 \le \gamma \le 1, \tag{15}$$

and $\chi(t,0) = 0 \quad \text{for } 0 < t < \infty$.

Note:

$$\chi(t,1) = \int_0^1 P_\gamma(t) d\gamma = P(t), \quad 0 \le t < \infty. \tag{16}$$

In order to describe $\chi(t,\gamma)$ for large (evolutionary) times when the variance of the pdf is small, we introduce a local co-ordinate transformation:

$$\begin{aligned} &\tau := \epsilon^2 t, \eta := (\gamma - \check{\gamma}(t))/\epsilon \quad \text{in } S. \\ \text{Note } &t = \tau/\epsilon^2 \quad \text{and} \quad \gamma = \check{\gamma}(t) + \epsilon\eta \quad \text{in } S. \end{aligned} \tag{17}$$

Here, we take small $\epsilon > 0$ as a scale for the standard deviation, so that the variance $v(t) \approx \epsilon^2$.

We define $\check{\gamma}(t)$ to be the maximum of $\partial\chi/\partial\gamma$ on $0 < \gamma < 1$. We expect $\check{\gamma}(t)$ to vary on the τ timescale, so that $\frac{d\check{\gamma}(t)}{dt} = \epsilon^2 \frac{d\check{\gamma}(\tau)}{d\tau}$. Then the partial derivatives of χ transform as follows:

$$\begin{aligned}\frac{\partial\chi}{\partial\gamma} &= \frac{\partial\chi}{\partial\tau}0 + \frac{\partial\chi}{\partial\eta}\frac{1}{\epsilon} = \frac{1}{\epsilon}\frac{\partial\chi}{\partial\eta},\\ \frac{\partial\chi}{\partial t} &= \frac{\partial\chi}{\partial\tau}\epsilon^2 + \frac{\partial\chi}{\partial\eta}\left(-\frac{1}{\epsilon}\frac{d\check{\gamma}(t)}{dt}\right),\\ \frac{\partial^2\chi}{\partial t\partial\gamma} &= \frac{\partial}{\partial\tau}\left(\frac{1}{\epsilon}\frac{\partial\chi}{\partial\eta}\right)\epsilon^2 + \frac{\partial}{\partial\eta}\left(\frac{1}{\epsilon}\frac{\partial\chi}{\partial\eta}\right)\left(-\frac{1}{\epsilon}\frac{d\check{\gamma}(t)}{dt}\right),\\ &= \epsilon\frac{\partial^2\chi}{\partial\tau\partial\eta} - \frac{d\check{\gamma}(\tau)}{d\tau}\frac{\partial^2\chi}{\partial\eta^2}.\end{aligned} \tag{18}$$

Under the transformation (17) the phenotype differential equation (14) becomes:

$$-\frac{d\check{\gamma}(\tau)}{d\tau}\frac{\partial^2\chi}{\partial\eta^2} + \epsilon\frac{\partial^2\chi}{\partial\tau\partial\eta} = \frac{1}{\epsilon}\frac{\partial\chi}{\partial\eta}f_P\left(\check{\gamma}(t)+\epsilon\eta;\frac{1}{\epsilon}\frac{\partial\chi}{\partial\eta}\right). \tag{19}$$

We expect the η derivatives of χ to become very small for large η when τ is order one. So we look for an expansion of (19) in the neighbourhood of $\check{\gamma}(t)$, that is η of order one when ϵ is small. We use the relationship between the mean and mode of the beta distribution (20):

$$\hat{\gamma}(t) - \check{\gamma}(t) = \frac{1-2\hat{\gamma}}{\hat{\gamma}(1-\hat{\gamma})}v + O(v^2), \tag{20}$$

when we move from the mode $\check{\gamma}$ to the mean $\hat{\gamma}$ with an error of order ϵ^4. To get an order one differential equation in (19) as $\epsilon \to 0$, we first define the equilibrium population $P^E(\tau)$ for the present value of $\hat{\gamma}(\tau)$:

$$\hat{f}_P(\hat{\gamma}(\tau);P^E(\tau)) = 0. \tag{21}$$

We construct the Taylor series expansion (to second order in ϵ as $\epsilon \to 0$):

$$\begin{aligned}T &:= \hat{f}_P(\hat{\gamma}(t);P^E(t)) + (\gamma-\hat{\gamma}(t))\frac{\partial\hat{f}_P}{\partial\hat{\gamma}} + \frac{1}{2}(\gamma-\hat{\gamma}(t))^2\frac{\partial^2\hat{f}_P}{\partial\hat{\gamma}^2},\\ &= \cancelto{0}{\hat{f}_P(\hat{\gamma}(t);P^E(t))} + \epsilon\eta\frac{\partial\hat{f}_P}{\partial\hat{\gamma}} + \frac{1}{2}\epsilon^2\eta^2\frac{\partial^2\hat{f}_P}{\partial\hat{\gamma}^2}.\end{aligned} \tag{22}$$

Next, we use T in (19) to find (to second order in ϵ):

$$-\frac{d\hat{\gamma}}{d\tau}\frac{\partial^2\chi}{\partial\eta^2} + \epsilon\frac{\partial^2\chi}{\partial\tau\partial\eta} = \frac{\partial\chi}{\partial\eta}\left\{\eta\frac{\partial\hat{f}_P}{\partial\hat{\gamma}} + \frac{1}{2}\epsilon\eta^2\frac{\partial^2\hat{f}_P}{\partial\hat{\gamma}^2}\right\}. \tag{23}$$

Finally, we expand χ in powers of ϵ:

$$\chi(t,\gamma) = \chi(\tau,\eta) = \chi^0(\tau,\eta) + \epsilon\chi^1(\tau,\eta) + \epsilon^2\chi^2(\tau,\eta) + \ldots. \tag{24}$$

Substituting (24) in (23) and collecting similar powers of ϵ yields:

$$-\frac{d\hat{\gamma}}{d\tau}\frac{\partial^2\chi^0}{\partial\eta^2} = \eta\frac{\partial\chi^0}{\partial\eta}\frac{\partial\hat{f}_P}{\partial\hat{\gamma}}, \tag{25}$$

$$-\frac{d\hat{\gamma}}{d\tau}\frac{\partial^2\chi^1}{\partial\eta^2} + \frac{\partial^2\chi^0}{\partial\tau\partial\eta} = \eta\frac{\partial\chi^1}{\partial\eta}\frac{\partial\hat{f}_P}{\partial\hat{\gamma}} + \frac{1}{2}\eta^2\frac{\partial^2\hat{f}_P}{\partial\hat{\gamma}^2}\frac{\partial\chi^0}{\partial\eta}. \tag{26}$$

We find a solution of (25) by separation of variables using:

$$\frac{d\hat{\gamma}}{d\tau} = \tilde{v}(\tau)\frac{\partial\hat{f}_P}{\partial\hat{\gamma}}. \tag{27}$$

Then, (25) becomes, for $\partial\hat{f}/\partial\hat{\gamma} \neq 0$:

$$\begin{aligned}\tilde{v}(\tau)\frac{\partial^2\chi^0}{\partial\eta^2} + \eta\frac{\partial\chi^0}{\partial\eta} &= 0,\\ \frac{\partial\chi^0}{\partial\eta} &= C(\tau)e^{-\eta^2/2\tilde{v}(\tau)},\\ \chi^0(\tau,\eta) &= C(\tau)\int_{-\check{\gamma}(\tau)/\epsilon}^{\eta} e^{-\eta^2/2\tilde{v}(\tau)}d\eta.\end{aligned} \tag{28}$$

We treat the χ^0 terms in (26) as a consistency equation for $\tilde{v}(\tau)$. Since χ^1 in (26) has the same form as χ^0 in (25) we then have:

$$\chi^0(\tau,\eta) + \epsilon\chi^1(\tau,\eta) = P(\tau)\int_{-\check{\gamma}(\tau)/\epsilon}^{\eta} e^{-\tilde{\eta}^2/2\tilde{v}(\tau)}d\tilde{\eta}\,/\sqrt{2\pi\tilde{v}(\tau)}. \tag{29}$$

Here, we integrate with respect to η at a fixed time using $P(t)$, the total population, to obtain (29).

Finally, we collect these expressions to define the eco-evolutionary population model:

$$\begin{aligned}\frac{1}{P}\frac{dP}{dt} &= \hat{f}_P + \frac{1}{2}v\frac{\partial^2\hat{f}_P}{\partial\hat{\gamma}^2},\\ \frac{d\hat{\gamma}}{dt} &= v\frac{\partial\hat{f}_P}{\partial\hat{\gamma}},\\ \frac{dv}{dt} &= \frac{2(1-2\hat{\gamma})}{\hat{\gamma}(1-\hat{\gamma})}v^2\frac{\partial\hat{f}_P}{\partial\hat{\gamma}} + v^2\frac{\partial^2\hat{f}_P}{\partial\hat{\gamma}^2}.\end{aligned} \tag{30}$$

Note that the expansion in powers of the small variance v is accurate to leading order on the evolutionary time scale that is proportional to $1/v$. This model contains a singularity in the coefficient of the first term of the variance equation when the trait mean $\hat{\gamma}$ approaches either bound, which leads to nonuniform behaviour in the variance. Hence, we seek the alternative representation for the variance, in terms of the trait differentiation Q. We substitute $\hat{\gamma}(1-\hat{\gamma})Q$ for v in (30) to give, after some simplification (Cropp and Norbury 2021), the eco-evolutionary population modelling framework (2).

We differentiate the identity:

$$v(t) = \hat{\gamma}(t)[1-\hat{\gamma}(t)]Q(t), \tag{31}$$

to get:

Table 2 Comparison of final states of the simulations of the phenotype model (1) and the simulation population model (6)-(8) shown in Figs. 1 and 4. Separate sub-population figures for the phenotype model in cases (b) and (d) were estimated by simply dividing the population at $\gamma = 0.5$

Figs 1, 4 cases*	P_1	$\hat{\gamma}_1$	v_1	P_2	$\hat{\gamma}_2$	v_2
Phenotype (a)	0.1014	0.5000	7 x10^{-4}	-	-	-
Population (a)	0.0498	0.4949	5 x10^{-4}	0.0498	0.5051	5 x10^{-4}
Phenotype (b)	0.4076	0.3067	1 x10^{-3}	0.4076	0.6933	1 x10^{-3}
Population (b)	0.4086	0.2887	2 x10^{-4}	0.4086	0.7113	2 x10^{-4}
Phenotype (c)	0.1155	0.5291	4 x10^{-4}	-	-	-
Population (c)	0.0510	0.5281	3 x10^{-4}	0.0635	0.5317	3 x10^{-4}
Phenotype (d)	0.2342	0.3252	8 x10^{-4}	0.5991	0.6922	2 x10^{-4}
Population (d)	0.2256	0.3007	3 x10^{-4}	0.6065	0.6864	2 x10^{-4}

*for cases (a) and (c) compare P_1 from the phenotype model with $P_1 + P_2$ from the population model, and $\hat{\gamma}_1$ of the phenotype model with $(\hat{\gamma}_1 + \hat{\gamma}_2)/2$ from the population model

$$\frac{dv}{dt} = [1 - 2\hat{\gamma}(t)]\frac{d\hat{\gamma}}{dt}Q(t) + \hat{\gamma}(t)[1 - \hat{\gamma}(t)]\frac{dQ}{dt}. \tag{32}$$

Then, we substitute for $\frac{dv}{dt}, \frac{d\hat{\gamma}}{dt}$ from (30); after some simplification, we have:

$$\frac{dQ}{dt} = Q^2\left\{[1 - 2\hat{\gamma}(t)]\frac{\partial \hat{f}}{\partial \hat{\gamma}} + \hat{\gamma}(t)[1 - \hat{\gamma}(t)]\frac{\partial^2 \hat{f}}{\partial \hat{\gamma}^2}\right\}. \tag{33}$$

Substituting (31) and (33) into (30) gives the eco-evolutionary population modelling framework (2). See Cropp and Norbury (2021, 2022) for the derivation of (2) using the moment generating method, together with the small variance asymptotic approximation of the third and fourth moments, giving closure with respect to $P, \hat{\gamma}$ and v in the small variance limit.

Extended eco-evolutionary population modelling framework

The canonical equations of the eco-evolutionary framework described in (2) for one evolving population (Cropp and Norbury 2021, 2022) may be extended to allow more than one population in an ecosystem to evolve. When two populations P_1, P_2, with the traits $\hat{\gamma}_1$, $\hat{\gamma}_2$ respectively, are involved then (2) becomes:

$$\begin{aligned}
\frac{dP_1}{dt} &= P_1\left(\hat{f}_1 + \frac{1}{2}\hat{\gamma}_1(1-\hat{\gamma}_1)Q_1\frac{\partial^2 \hat{f}_1}{\partial \hat{\gamma}_1^2} + \frac{1}{2}\hat{\gamma}_2(1-\hat{\gamma}_2)Q_2\frac{\partial^2 \hat{f}_1}{\partial \hat{\gamma}_2^2}\right),\\
\frac{dP_2}{dt} &= P_2\left(\hat{f}_2 + \frac{1}{2}\hat{\gamma}_2(1-\hat{\gamma}_2)Q_2\frac{\partial^2 \hat{f}_2}{\partial \hat{\gamma}_2^2} + \frac{1}{2}\hat{\gamma}_1(1-\hat{\gamma}_1)Q_1\frac{\partial^2 \hat{f}_2}{\partial \hat{\gamma}_1^2}\right),\\
\frac{d\hat{\gamma}_1}{dt} &= \hat{\gamma}_1(1-\hat{\gamma}_1)Q_1\frac{\partial \hat{f}_1}{\partial \hat{\gamma}_1},\\
\frac{d\hat{\gamma}_2}{dt} &= \hat{\gamma}_2(1-\hat{\gamma}_2)Q_2\frac{\partial \hat{f}_2}{\partial \hat{\gamma}_2},\\
\frac{dQ_1}{dt} &= Q_1^2\left((1-2\hat{\gamma}_1)\frac{\partial \hat{f}_1}{\partial \hat{\gamma}_1} + \hat{\gamma}_1(1-\hat{\gamma}_1)\frac{\partial^2 \hat{f}_1}{\partial \hat{\gamma}_1^2}\right),\\
\frac{dQ_2}{dt} &= Q_2^2\left((1-2\hat{\gamma}_2)\frac{\partial \hat{f}_2}{\partial \hat{\gamma}_2} + \hat{\gamma}_2(1-\hat{\gamma}_2)\frac{\partial^2 \hat{f}_2}{\partial \hat{\gamma}_2^2}\right).
\end{aligned} \tag{34}$$

To extend the single population model to two populations, we use a double Taylor series expansion in the moment-based methodology and assume that the pdfs associated with $\hat{\gamma}_1$ and $\hat{\gamma}_2$ are linearly independent so that the covariance terms disappear. The next refinement of the two population modelling framework would be to include the covariance terms.

Numerical simulations

The population model (6), (34), was solved numerically as a coupled ordinary differential equation system using an adaptive step size 4–5th order Runge–Kutta numerical integration technique with the error tolerances set to machine epsilon (10^{-14}). The model was integrated for 200-time steps, notionally generations, which were sufficient to arrive at the long-term properties of the system. We used small variance beta distributions for the initial conditions of the sub-populations P_1 and P_2, with $\alpha_1 = 20, \beta_1 = 180$, and $\alpha_2 = 22, \beta_2 = 178$. Only the summary statistics $\hat{\gamma} = \frac{\alpha}{\alpha+\beta}$ and $Q = \frac{1}{\alpha+\beta+1}$ were used in the initial conditions of the population model. The initial population sizes obey $P_1 + P_2 = P$.

We estimated the shape parameters of the phenotype distributions of the model from the mean $\hat{\gamma}$ and variance v for each of the sub-populations using:

$$\alpha = \hat{\gamma}\left(\frac{\hat{\gamma}(1-\hat{\gamma})}{v} - 1\right), \quad \beta = (1-\hat{\gamma})\left(\frac{\hat{\gamma}(1-\hat{\gamma})}{v} - 1\right). \tag{35}$$

We then produced a phenotype distribution for the model at each time step by creating a beta distribution using the shape parameters calculated for that time step. A phenotype distribution for the whole population was then created by adding the distributions of the sub-populations. The distributions were calculated using 101 phenotypes.

Final distributions

The correspondence between the distributions predicted by the phenotype and population models throughout the

simulations is qualitatively good (cf. Figures 1 and 4). We quantified the correspondence of the long-term results of the models by comparing the sub-population sizes and the means and variances of the traits at the ends of the simulations. These comparisons are shown in Table 2.

For each phenotype simulation, we use $P_i(t = 200)/P(t = 200)$ as a probability density function to calculate the mean $\hat{\gamma}(t = 200)$ and variance $v(t = 200)$ of the solutions in Fig. 1.

The comparison of the final distributions of the phenotype and population models reveals a very good correspondence between the two models. The greatest difference between the model predictions is 8% (case (d), $\hat{\gamma}_1$), but most errors are small, with several less than 1%.

We also note the similarity between the results of these models with those of the model of Meszena et al. (2005) which, although produced by a phenotype model with a quite different fitness function, has a fitness surface with a very similar shape to that of the single version of the population model (Fig. 2).

Bifurcation dynamics

To appreciate the details of the changes taking place in the system, we examine the properties of the ecological $\{P_1, P_2\}$ and evolutionary $\{\hat{\gamma}_1, \hat{\gamma}_2\}$ phase planes at various points in the integration. Note that the phase space of the system is six-dimensional, so the two-dimensional slices that we examine change as other state variables change. We do not show the $\{Q_1, Q_2\}$ phase plane as these quantities generally tend to zero, apart from the brief increases noted above that correlate with evolutionary branching. Their phase planes consist only of the zero isoclines $Q_1 = 0$ and $Q_2 = 0$, for Q_1 and Q_2 small and positive, and a single always stable equilibrium point at $\{Q_1^* = 0, Q_2^* = 0\}$ - this point is always neutrally stable under linear theory.

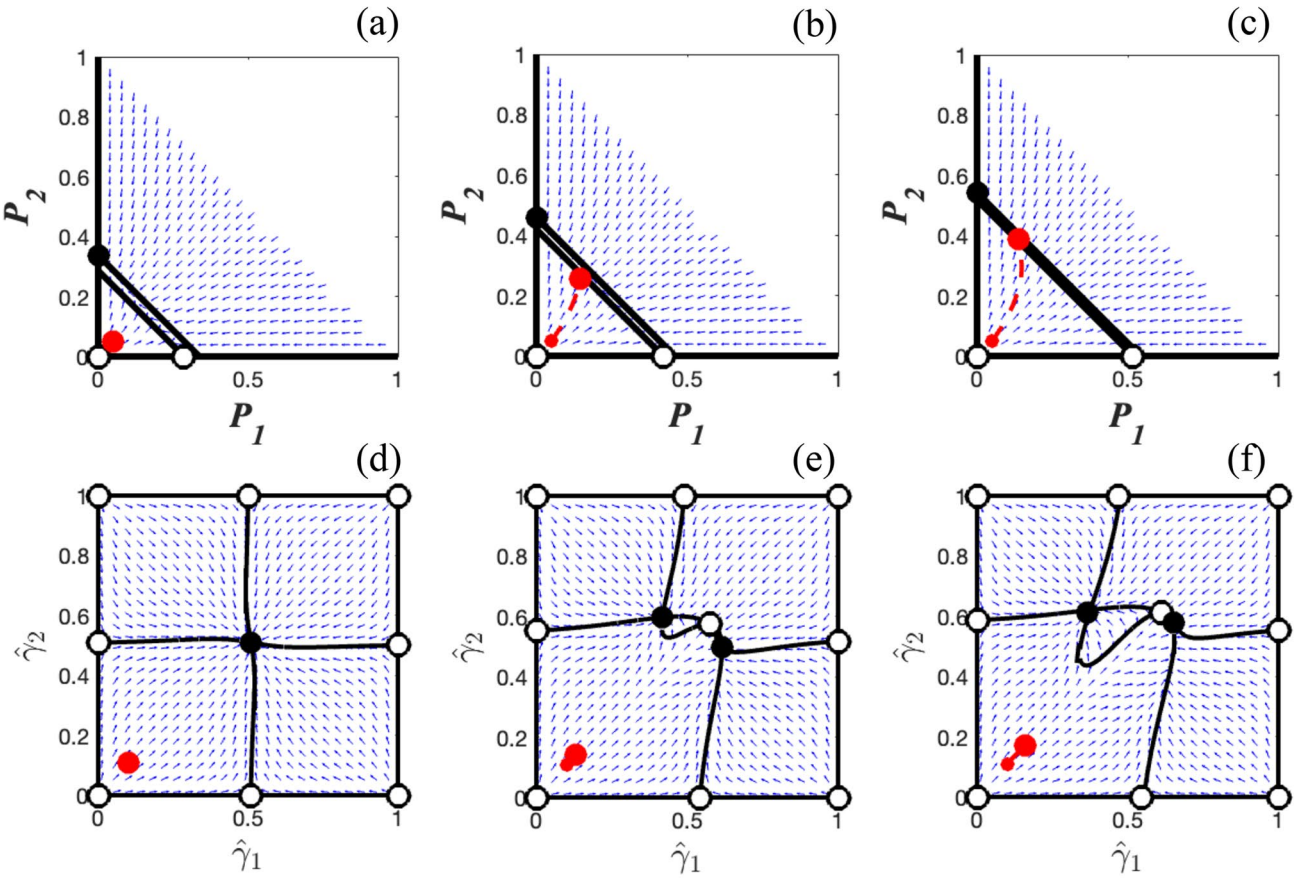

Fig. 10 The phase planes of the population model (6)-(8): the $\{P_1, P_2\}$ spaces (top), and the $\{\hat{\gamma}_1, \hat{\gamma}_2\}$ spaces (bottom) at time 1 **a**, **d**, 10 **b**, **e** and 20 **c**, **f** of the integration shown in Figs. 7 and 8. Zero isoclines are shown by black lines, stable equilibrium points by black dots, and unstable ones by white dots. The stability classifications only refer to stability properties within the two-dimensional slices of the six-dimensional phase space. The blue arrows show the vector field, and the dashed red lines show the dynamics of the system from the start of the integration (small red dot near the origin) to the current time (large red dot). Note that the details of each phase plane depend upon the other, that is, changes in $\hat{\gamma}_1$ and $\hat{\gamma}_2$ values affect the $\{P_1, P_2\}$ phase plane and *vice versa*. The phase planes shown are therefore specific to the parameter set and initial conditions. Separatrices in the evolutionary phase space sections are not shown in these diagrams but may be inferred from the vector fields

We consider a number of snapshots that reveal important changes of the dynamic properties of the system. Note that the stability classifications applied to the equilibrium points in the phase plane sections only apply to the stability in the dimensions of the section - they do not consider the stability of the points in the full six-dimensional space. Nevertheless, these planar stabilities appear useful in determining the dynamics of the system.

Figure 10 shows the ecological phase planes for time 1 (a, d), for time 10 (b, e), and for time 20 (c, f). The ecological phase plane in Fig. 10a shows that the system starts in a classic competitive exclusion scenario, where in the absence of evolution, P_2 will dominate and P_1 will go extinct. The evolutionary phase plane (d) reveals that the system begins in a state that suggests that no evolutionary branching will occur - the ecology sees only a stable equilibrium state in the evospace where $\hat{\gamma}_1 = \hat{\gamma}_2$. As the integration progresses P_2 initially dominates the ecosystem and P_1 falls to low levels, which leads to significant changes in the evolutionary phase plane (e and f).

Note that the $\hat{f}_1 = 0$ and $\hat{f}_2 = 0$ isoclines in Figs. 10 and 11 are almost coincident, and remain so until the sub-populations branch in evolutionary space to form sub-populations with different mean trait values. This will always be the case in eco-evolutionary population models of this type as the two initial populations differ only minimally in their mean trait values. The two nearly coincident zero isoclines form a zone where both $\hat{f}_1$ and $\hat{f}_2$ are near zero, but are not necessarily near a stable equilibrium point. This creates a region that we refer to as the "swamp" where the populations slowly move through a morass of near-zero rates of change. In this morass the curvature of the fitness landscape may drive ecological change. This is discussed further in the "The non-equilibrium dynamics zone" section.

Figure 11 then shows a rapid transition to P_1 dominating the ecology, which occurs around time 40 (Fig. 14). The very rapid exchange of dominance between P_2 and P_1, associated with the two transcritical bifurcations on the boundaries in quick succession, provides the interesting dynamic of the system state and the stable equilibrium point approaching each other from opposite sides of the ecological phase plane. However, although unusual, these are simple changes in the dynamical system compared to the changes that occur in the evolutionary phase plane.

The trajectory shows that while the populations are changing, the properties of the system change little. This

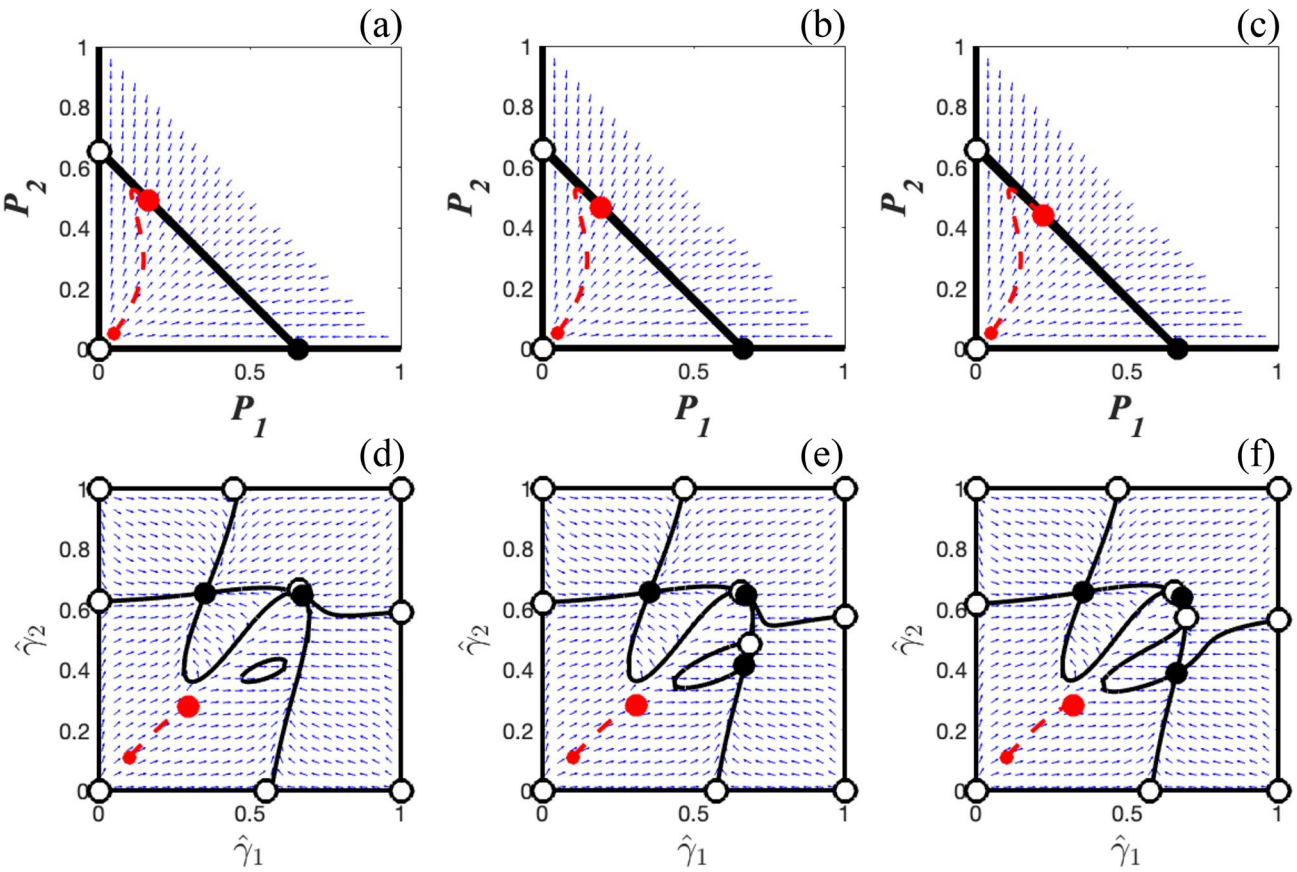

Fig. 11 The phase planes of the population model (6)–(8): the $\{P_1, P_2\}$ spaces (top), and the $\{\hat{\gamma}_1, \hat{\gamma}_2\}$ spaces (bottom) at time 80 **a**, **d**), 86 **b**, **e**, and 90 **c**, **f** of the integration shown in Fig. 7. Details as for other phase plane diagrams

apparent evolutionary dead-end does not last long however. While the ecology is embarking on its apparently pre-determined extinction scenario, significant changes are occurring in the evospace (d, e, and f). The zero-isoclines begin to buckle, and undergo a bifurcation. The stable evolutionary equilibrium point splits into a pair of stable and an unstable set of equilibrium points, the latter introducing a separatrix into the section through the evolutionary domain, which is then evident in various forms through the remainder of the integration. The effect of this separatrix in six dimensions is ambiguous, as the final evolutionary phase plane (Fig. 7d) appears to show the trajectory crossing the separatrix in the evolutionary phase plane.

The state of the evospace then remains relatively unchanged, from time 20 in Fig. 10 to time 80 in Fig. 11, while the ecology, having embarked upon its path to the extinction of P_1, has responded to the very subtle changes in the evolutionary side where the mean trait value of the population has increased from $\hat{\gamma}_1 = 0.10 = \hat{\gamma}_2$ to $\hat{\gamma}_1 \approx 0.36, \hat{\gamma}_2 \approx 0.34$. This change has facilitated P_1's competitive ability with P_2, and it now has become the favoured competitor. Consequently, the trajectory in the ecological space has turned away from P_2, and P_1 is beginning to dominate.

The equilibrium points in the evospace have changed position only slightly during this time, but the zero isoclines have become more buckled, and a further closed loop zero isocline associated with $\hat{f}_1 = 0$ has appeared. The new isocline does not initially create any new equilibrium points, but by time 85 it has expanded until it is tangent to another zero isocline, and a second stable equilibrium point is created in a blue sky bifurcation. This isocline then further expands and merges with the other $\hat{f}_1$ zero isocline. This bifurcation introduces a stable equilibrium point into the same section of the phase plane as the current state of the system, providing an attractor for the system. This attractor is associated with two different phenotype groups, P_1 with $\hat{\gamma}_1 \approx 0.6$ and P_2 with $\hat{\gamma}_2 \approx 0.4$.

The next significant changes in the evospace happen at around time 116, when the two lobes of the zero isoclines, which are near the state of the system in Fig. 11c, come together to form an unstable equilibrium point at $\hat{\gamma}_1 \approx 0.4, \hat{\gamma}_2 \approx 0.4$. The appearance of this saddle point

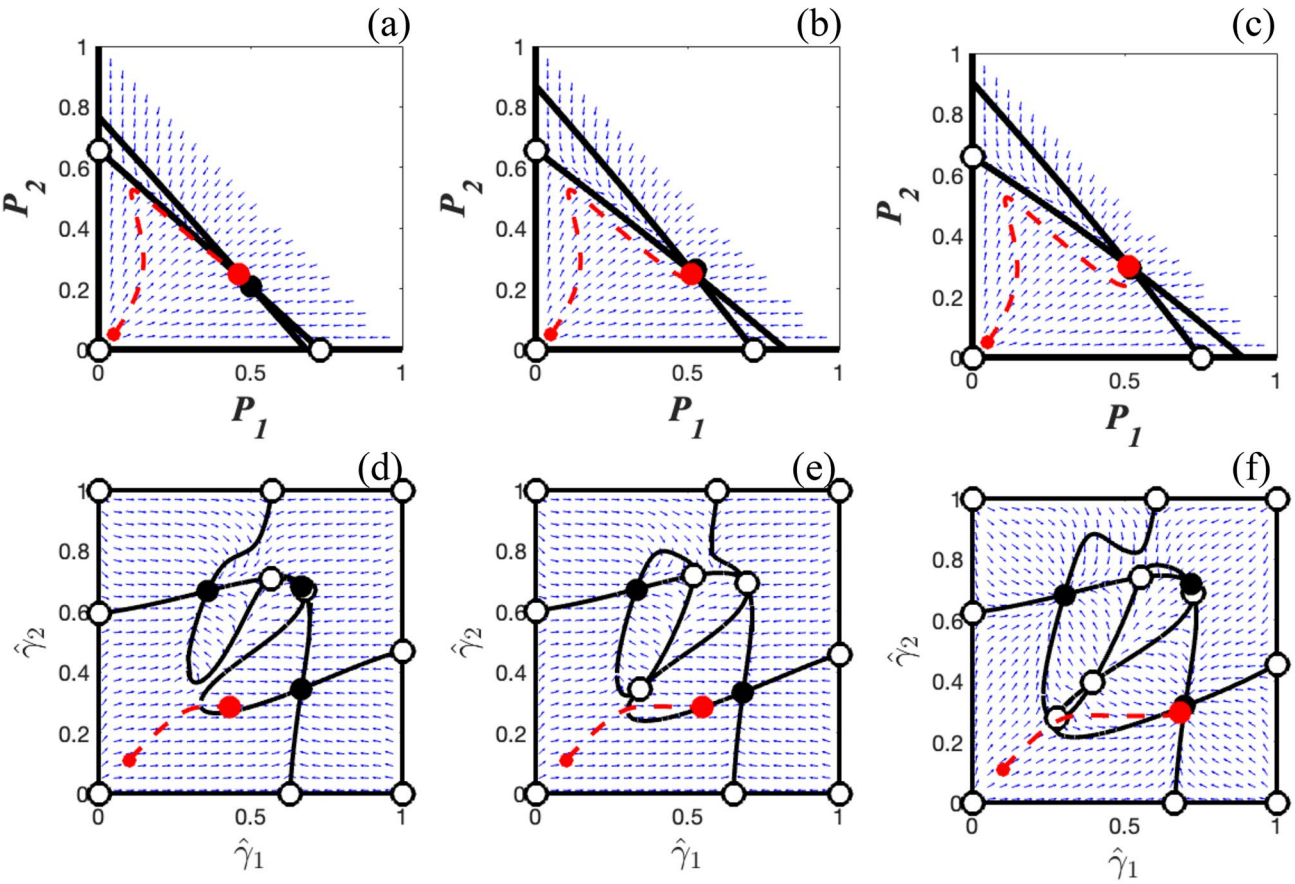

Fig. 12 The phase planes of the population model (6)-(8): the $\{P_1, P_2\}$ spaces (top), and the $\{\hat{\gamma}_1, \hat{\gamma}_2\}$ spaces (bottom) at time 108 **a**, **d**, 116 **b**, **e**, and 160 **c**, **f** of the integration shown in Fig. 7. The phase planes at the equilibrium state of the system are shown in Fig. 7. Details as for other phase plane diagrams

confirms that evolutionary branching is occurring, and directs the trajectory of the system towards the stable equilibrium at $\hat{\gamma}_1 \approx 0.6, \hat{\gamma}_2 \approx 0.3$. Interestingly, evolutionary branching appears to be initiated before the appearance of the saddle point, as Fig. 11d shows the trajectory in the evospace deflecting at time 108 before the saddle point is established.

Figures 7 to 12 provide snapshots of key moments in the eco-evolutionary dynamics, but are also useful for looking at the overall dynamics of the internal equilibrium points. These are shown in Fig. 14, and reveal marked differences in the complexity of the ecological and evolutionary dynamics. Figures 10 to 11 show that initially the $\{P_1^* = 0, P_2^* \approx 0.4\}$ equilibrium point is stable, but by time 80 the opposite point $\{P_1^* = 0.7, P_2^* = 0\}$ is stable (see also Figs. 10 and 11). Figure 14a, b shows that the transition between these two states occurs at around time 40 and is very rapid, so the system effectively does not have a stable attracting internal equilibrium point until a transcritical bifurcation that occurs at around time 100. The two boundary points control the ecological dynamics for the first half of the integration, and while (b) shows the internal point controls the second half, (a) suggests that the net effect on the ecological dynamics is comparatively small.

Robustness of results

A reviewer of this manuscript queried the robustness of our results to different bifurcation parameters, asymmetry, and inclusion of additional terms in the denominator of the competition term. We tested the framework's robustness by including the following growth term $\hat{f}_i$ into our modelling framework (7) as suggested by the reviwer:

$$\hat{f}_i = \frac{\mu\hat{\gamma}_i(1-\hat{\gamma}_i)N}{(N+\kappa)} - \frac{P_i}{\eta + \rho(\hat{\gamma}_i - \hat{\gamma}_C)^2} - \frac{P_j}{\eta + \rho(\hat{\gamma}_i - \hat{\gamma}_C)^2 + \omega(\hat{\gamma}_i - \hat{\gamma}_j)^2 + \alpha(\hat{\gamma}_i - \hat{\gamma}_j)} - \sigma, \tag{36}$$

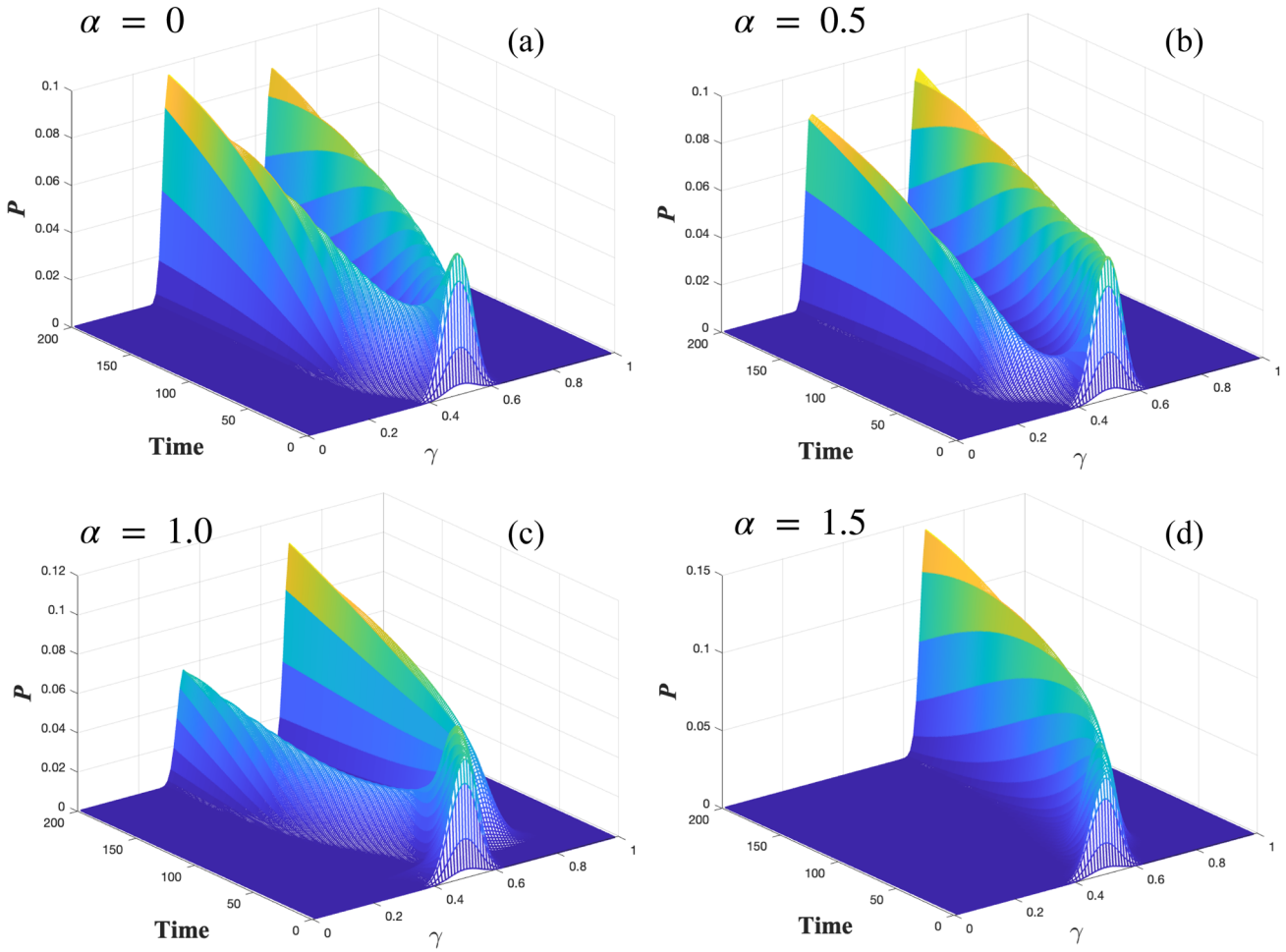

Fig. 13 Distributions of phenotypes produced by the two sub-population model using the reviewer's suggestion for $\hat{f}_i$ (36) together with equation (7). Note the simulations use the same parameter values and initial conditions as those shown in Fig. 4

for $i,j = 1,2$ ($i \neq j$). The appearance of the α term ensures that certain derivatives that are important in AD have different values.

Phenotype distributions obtained by the revised model using (36) with various values of α are provided in Fig. 13. Panel (a) of Fig. 13 shows the results for $\alpha = 0$ - these are identical to panel (b) of Fig. 4 in the original ms and indicate that we have not introduced any errors into the code when modifying the model.

As the value of α is increased, in panels (b-d), its effect becomes clear. It has little effect at low values (around 0.5) but as it increases it apparently biases the fitness landscape and eliminates the evolutionary branching (d). Note that the values of α used in these simulations are commensurate with the values of the other parameters in the denominator of the term: $\eta = 0.5$, $\rho = 4$, and $\omega = 6$.

These simulations suggest that the eco-evolutionary modelling framework we propose is robust. The additional example model copes with additional terms, different forms of asymmetry of the fitness landscape, and different parameters to produce different bifurcations. However, the model consistently produces plausible solutions. Note that the bifurcation previously explored by manipulating σ is reproduced here by varying α.

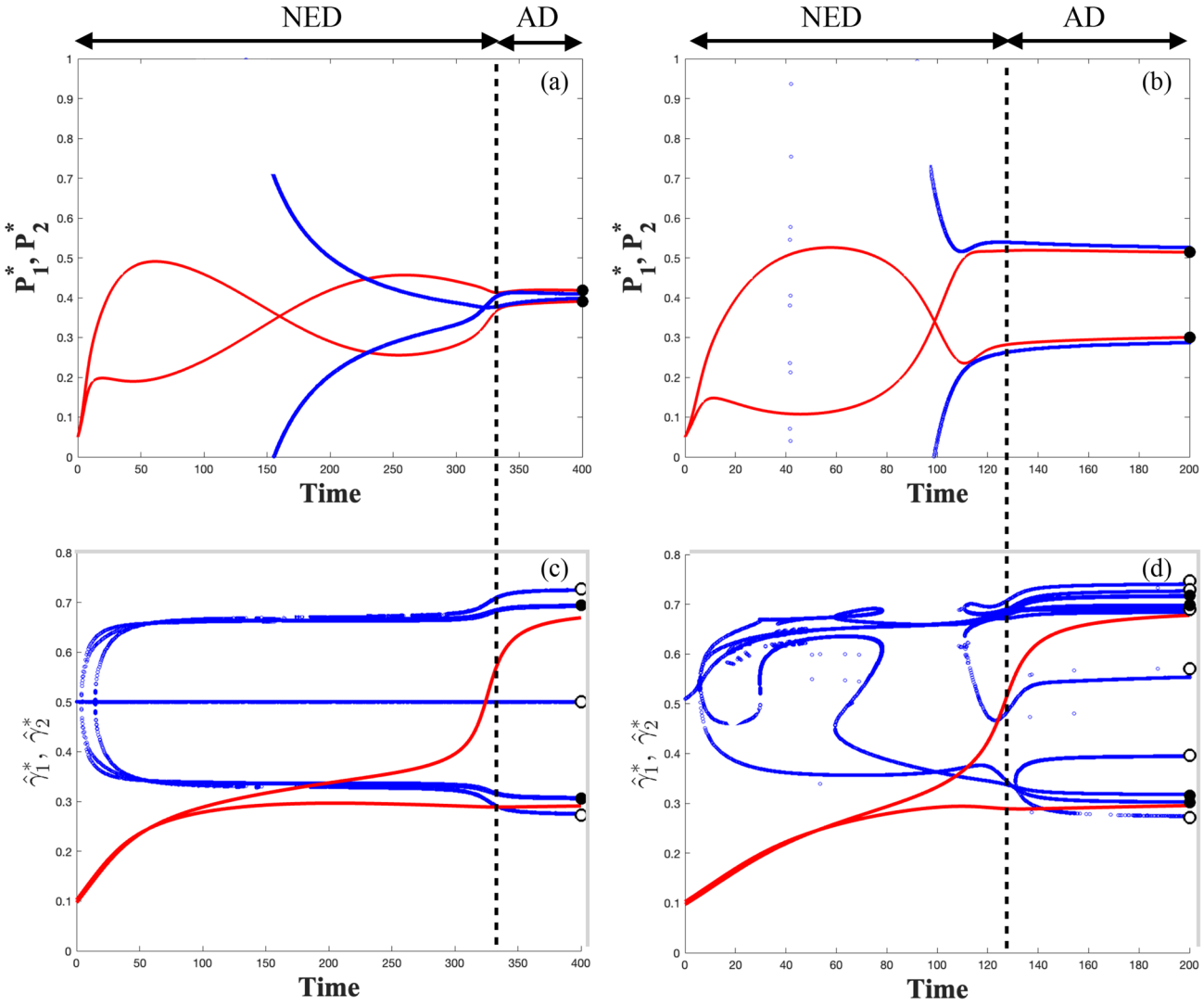

Fig. 14 Time series of the internal equilibrium points shown in the ecology (**a** and **b**), and the evolutionary spaces (**c** and **d**) of the population model (6)-(8) for symmetric (a and c) and asymmetric (b and d) fitness landscapes. The results in (**b**) and (**d**) are for the integration shown in Figs. 8 to 12. This uses the same parameter values as the other simulations but uses the initial conditions $P_1 = 0.025 = P_2$, $\hat{\gamma}_1 = 0.0975$, $\hat{\gamma}_2 = 0.1025$ and $Q_1 = 0.005 = Q_2$. The P_1, P_2, $\hat{\gamma}_1$ and $\hat{\gamma}_2$ trajectories are shown by red lines, and the dynamics of the equilibrium points P_1^*, P_2^*, $\hat{\gamma}_1^*$ and $\hat{\gamma}_2^*$ by the blue dots. The black and white dots show the locations of the stable and unstable interior equilibrium points at the end of the integration. Boundary equilibrium points are not shown. The NED and AD zones are differentiated by the vertical dashed lines and labelled at the top of the diagram. Details of the changes in the vector field sections through the ecological and evolutionary spaces at key points in Fig. 14 are provided in Appendix "Bifurcation dynamics" section

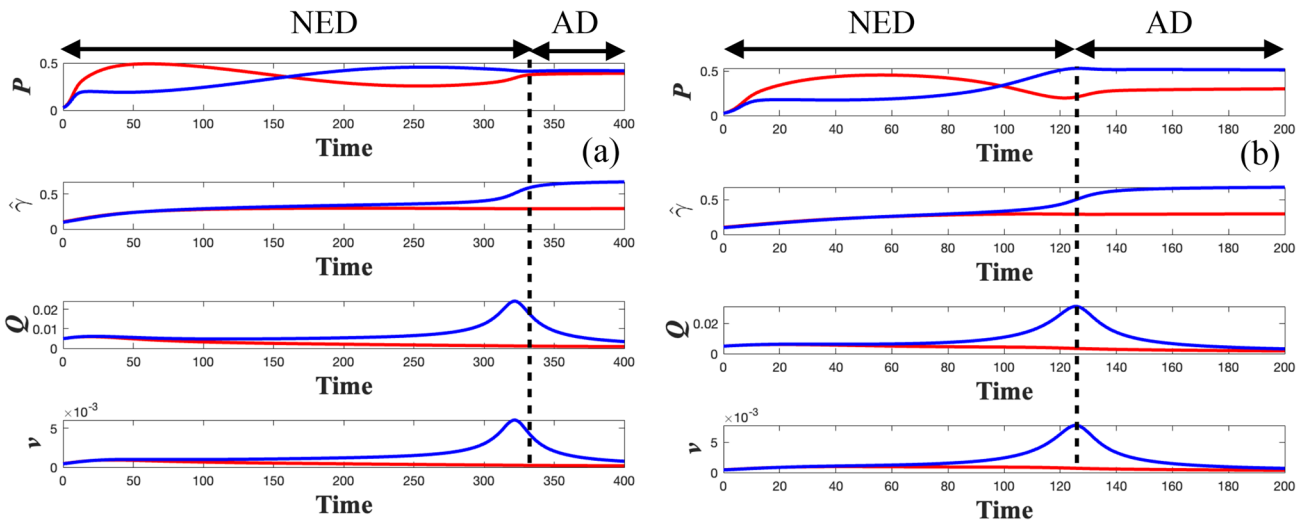

Fig. 15 The time series of state variables for integrations of the eco-evolutionary population model (6)-(8) shown in Fig. 14. The time series shown are the population size in each of the sub-populations (P, top), the average phenotype value for each sub-population ($\hat{\gamma}$, second panel), the trait differentiation (Q, third panel), and the trait variance of each sub-population (v, bottom). Time series data for P_1 is shown by the red line, and P_2 by the blue line in each case. The P and $\hat{\gamma}$ data are repeated from Fig. 14. The different dynamical regions identified in Fig. 14 are included in these plots. Note the peaks in Q and v may lie within or without the AD zone

The non-equilibrium dynamics zone

Sections through the solution space at the end of the integration such as Fig. 8 do not provide complete pictures of the dynamics of the system, as implied by the trajectories, that are generally inconsistent with the final vector fields. Figure 14 shows the changes over time in the locations of the interior equilibrium points of the ecological and evolutionary spaces for the symmetric (a and c) and asymmetric (b and d) fitness landscapes of the two sub-population model (6), (34).

The ecological spaces show that for much of the evolution of the system, the state of the ecology is far from equilibrium - it is only towards the ends of the simulations ($t > 340$ and $t > 125$ respectively) that the ecology nears a stable equilibrium and here our results approximate those of AD. However, the evolutionary spaces show that significant changes to the evolutionary properties of the system have occurred prior to the system reaching the AD zone. In both cases, many bifurcations of equilibrium points have occurred, with points appearing and disappearing in various bifurcations, as well as points moving position. Here, our dynamics will significantly differ from interim states predicted by AD.

The results in Fig. 14 allow the identification of two dynamical zones that may apply to eco-evolutionary systems:

- a Non-Equilibrium Dynamics zone (NED) where the ecological state variables are not near equilibrium, and the ecological and evolutionary variables may change by similar magnitudes (see Fig. 10b to Fig. 12a in Appendix "Bifurcation dynamics");
- an Adaptive Dynamics zone (AD) where the ecology is near and approaching a stable ecological equilibrium point on $\{\hat{f} = 0\}$ and the ecological state variables change by smaller magnitudes than the evolutionary state variables (see Fig. 12a to c in Appendix "Bifurcation dynamics" section).

The AD zone is readily identified as the region where the trajectories (red lines) lie close to the stable internal equilibrium point (blue dots). This region extends from generation 330 to 400 in the symmetric fitness case (a and c), and from 125 to 200 in the asymmetric fitness case (b and d). The temporal extents of the two zones evident in Fig. 14b, d may be confirmed in Figs. 10 to 12 in Appendix "Bifurcation dynamics" section.

Figure 14 provides an interesting comment on the dynamics of evolutionary branching in eco-evolutionary systems. For nearly half of the integration, while substantial eco-evolutionary changes are taking place, the system provides little indication that evolutionary branching may occur in the future. It is the rapid appearance of the saddle point at $\hat{\gamma}_1 \approx 0.30, \hat{\gamma}_2 \approx 0.30$ that introduces the prospect of evolutionary branching, after which the system is characterised as one in which evolutionary branching is possible.

Note that the extent of the NED zone may depend on the specific system being examined. Figure 14a, c reveals that the NED zone in this case extends for about 320 generations, rather than the approximately 100 generations in Fig. 14c, d. The only difference between these two simulations is that

the fitness landscape is symmetrical ($\hat{\gamma}_C = 0.50$) in (a and c) and asymmetrical ($\hat{\gamma}_C = 0.45$) in (b and d).

Finally, the time series in Fig. 15 show clearly the key role of a spike in Q associated with the onset of evolutionary branching, as previously observed in other solutions shown in Fig. 7. The spikes in Q may lie within the AD zone, as in the asymmetric case (b), or outside the AD zone, as in the symmetric case (a). However, Q has little influence on the equilibrium state of the system, as it reduces to a small positive value after the evolutionary branching has occurred, suggesting that AD could produce similar equilibrium solutions to our eco-evolutionary model.

Acknowledgements The authors wish to thank Gyuri Barabás for comments and suggestions made on an early draft of this manuscript, and three very conscientious reviewers who commented on a later version.

Author contribution John Norbury derived the new equations; Roger Cropp conducted the numerical analyses; both authors contributed to the writing of the manuscript.

Funding Open Access funding enabled and organized by CAUL and its Member Institutions The authors declare that no funds, grants, or other support were received during the preparation of this manuscript.

Declarations

Ethics approval Not applicable.

Consent to participate Not applicable.

Conflict of interest The authors declare no competing interests.

References

Abrams P (2001) Modelling the adaptive dynamics of traits involved in inter- and intraspecific interactions: an assessment of three methods. Ecol Lett 4:166–175

Abrams P, Matsuda H, Harada Y (1993) Evolutionarily unstable fitness maxima and stable fitness minima of continuous traits. Evol Ecol 7:465–487

Beaufort L, Bolton C, Sarr A, Sucheras-Marx B, Rosenthal Y, Donnadieu Y, Barbarin N, Bova S, Cornuault P, Gally Y, Gray E, Mazur J, Tetard M (2022) Cyclic evolution of phytoplankton forced by changes in tropical seasonality. Nature 601(7077):79–84

Behrenfeld M, Bisson K, Boss E, Gaube P, Karp-Boss L (2022) Phytoplankton community structuring in the absence of resource-based competitive exclusion. PLoS ONE 17(9):e0274183

Bell G (2017) Evolutionary rescue. Annu Rev Ecol Evol Syst 48:605–627

Bullock H, Luo H, Whitman W (2017) Evolution of dimethylsulfoniopropionate metabolism in marine phytoplankton and bacteria. Front Microbiol 8:1–17. https://doi.org/10.3389/fmicb.2017.00637

Charlson R, Lovelock J, Andreae M, Warren S (1987) Oceanic phytoplankton, atmospheric sulphur, cloud albedo and climate. Nature 326:655–661

Cortez M (2018) Genetic variation determines which feedbacks drive and alter predator-prey eco-evolutionary cycles. Ecol Monogr 88(3):353–371

Cropp R, Norbury J (2015) Population interactions in ecology: a rule-based approach to modeling ecosystems in a mass-conserving framework. SIAM Rev 57(3):437–465

Cropp R, Norbury J (2021) The eco-evolutionary modelling of populations and their traits using a measure of trait differentiation. J Theor Biol 531(110893):1–24

Cropp R, Norbury J (2022) Predator-prey evolution from an eco-evolutionary trade-off model: the role of trait differentiation. Bull Math Biol 84(50):s11538–022–01004–8

Debarre F, Otto S (2016) Evolutionary dynamics of a quantitative trait in a finite asexual population. Theor Popul Biol 108:75–88

Della Rossa F, Dercole F, Landi P (2015) The branching bifurcation of adaptive dynamics. Int J Bifurcat Chaos. https://doi.org/10.1142/S0218127415400015

Dercole F, Della Rossa F, Landi P (2016) The transition from evolutionary stability to branching: a catastrophic evolutionary shift. Sci Rep 6(26310):1–8

Dieckmann U, Doebeli M (1999) On the origin of species by sympatric speciation. Nature 400:354–357

Dieckmann U, Law R (1996) The dynamical theory of coevolution: a derivation from stochastic ecological processes. J Math Biol 34:579–612

Fussman G, Loreau M, Abrams P (2007) Eco-evolutionary dynamics of communities and ecosystems. Funct Ecol 21(3):465–477

Geritz S, Metz J, Kisdi E, Meszena G (1997) Dynamics of adaptation and evolutionary branching. Phys Rev Lett 78(10):2024–2027

Geritz S, Kisdi E, Meszena G, Metz J (1998) Evolutionarily singular strategies and the adaptive growth and branching of the evolutionary tree. Evol Ecol 12:35–57

Grant P, Grant B (2006) Evolution of character displacement in Darwin's finches. Science 313(5784):224–226

Hinners J, Kremp A, Hense I (2017) Evolution in temperature-dependent phytoplankton traits revealed from a sediment archive: do reaction norms tell the whole story? Proc R Soc B 284:20171888

Hui C, Richardson D, Landi P, Minoarivelo H, Roy H, Latombe G, Jing X, CaraDonna P, Gravel D, Beckage B, Molofsky J (2021) Trait positions for elevated invasiveness in adaptive ecological networks. Biol Invasions 23:1965–1985

Irwin A, Finkel Z, Muller-Karger F, Ghinaglia L (2015) Phytoplankton adapt to changing ocean environments. PNAS 112(18):5762–5766

Kisdi E (1999) Evolutionary branching under asymmetric competition. J Theor Biol 197:149–162

Klauschies T, Coutinho R, Gaedke U (2018) A beta distribution-based moment closure enhances the reliability of trait-based aggregate models for natural populations and communities. Ecol Model 381:46–77

Lancelot C, Allen J, Archer S, Bopp L, Deal C, Elliott S, Jin M, Malin G, Schoemann V, Simo R, Six K, Stefels J (2010) A first appraisal of prognostic ocean DMS models and prospects for their use in climate models. Global Biogeochem Cycles 24(GB3021):1–13. https://doi.org/10.1029/2009GB003721

Lande R (1976) Natural selection and random genetic drift in phenotype evolution. Evolution 30:314–334
Law R, Marrow P, Dieckmann U (1997) On evolution under asymmetric competition. Evol Ecol 11:485–501
Le Gland G, Vallina SM, Smith SL, Cermeno P (2021) Spead 1.0 - simulating plankton evolution with adaptive dynamics in a two-trait continuous fitness landscape applied to the sargasso sea. Geosci. Model Dev 14:1949–1985
Lion S, Sasaki A, Boots M (2023) Extending eco-evolutionary theory with oligomorphic dynamics. Ecol Lett 00:1–25
Loreau M (2010) From populations to ecosystems, Vol. 46 of monographs in population biology. Princeton University Press, Woodstock, Oxfordshire
Meszena G, Gyllenberg M, Jacobs F, Metz J (2005) Link between population dynamics and dynamics of Darwinian evolution. Phys Rev Lett 95(078105):1–4
Metz JA, Nisbet R, Geritz S (1992) How should we define 'fitness' for general ecological scenarios? Trends Ecol Evol 7(6):198–202
Metz J, Geritz S, Meszena G, Jacobs F, van Heerwaarden J (1996) Adaptive dynamics: a geometrical study of the consequences of nearly faithful reproduction. Elsevier Science, North-Holland, pp 183–231
Mullon C, Lehmann L (2019) An evolutionary quantitative genetics model for phenotypic (co)variances under limited dispersal, with an application to socially synergistic traits. Evolution 73(9):1695–1728
Naaman M (2021) On the tight constant in the multivariate Dvoretzky-Kiefer-Wolfowitz inequality. Statist Probab Lett 173:109088
Padfield D, Yvon-Durocher G, Buckling A, Jennings S, Yvon-Durocher G (2017) Rapid evolution of metabolic traits explains thermal adaptation in phytoplankton. Ecol Lett 19(2):133–142
Patel S, Burger R (2019) Eco-evolutionary feedbacks between prey densities and linkage disequilibrium in the predator maintain diversity. Evolution 73(8):1533–1548
Pelletier F, Garant D, Hendry A (2009) Eco-evolutionary dynamics. Phil Trans Roy Soc B 364:1483–1489
Rubin I, Ispolatov I, Doebeli M (2021) Evolution to alternative levels of stable diversity leaves areas of niche space unexplored. PLoS Comput Biol 17(7):e1008650
Sasaki A, Dieckmann U (2011) Oligomorphic dynamics for analyzing the quantitative genetics of adaptive speciation. J Math Biol 63:601–635
Schoener T (2011) The newest synthesis: understanding the interplay of evolutionary and ecological dynamics. Science 331:426–429
Senthilnathan A, Gavrilets S (2021) Ecological consequences of intraspecific variation in coevolutionary systems. Am Nat 197(1):1–17
Stephens M (1974) EDF statistics for goodness of fit and some comparisons. J Am Stat Assoc 69(347):730–737
Villa Martin P, Hidalgo J, Rubio de Casas R, Munoz M (2016) Eco-evolutionary model of rapid phenotypic diversification in species-rich communities. PLoS Comput Biol 12(10):e1005139. https://doi.org/10.1371/journal.pcbi.1005139
Vitousek P, Matson P (2012) Nutrient cycling and biogeochemistry. In: Levin S (ed) The Princeton guide to ecology. Princeton University Press, Princeton New Jersey, pp 330–339
Wakano J, Iwasa Y (2013) Evolutionary branching in a finite population: deterministic branching vs. stochastic branching. Genetics 193(1):229–241
Ward B, Collins S, Dutkiewicz S, Gibbs S, Bown P, Ridgwell A, Sauterey B, Wilson J, Oschlies A (2019) Considering the role of adaptive evolution in models of the ocean and climate system. J Adv Model Earth Syst. https://doi.org/10.1029/2018MS001452
Waxman D, Gavrilets S (2005) 20 questions on adaptive dynamics. J Evol Biol 18:1139–1154
Wong T (2019) The evolutionary contingency thesis and evolutionary idiosyncrasies. Biol Philos. https://doi.org/10.1007/s10539-019-9684-0